Review article

Control of ZnO nanowires growth in flexible perovskite solar cells: A mini-review

Karthick Sekar [a],[**], Raphaël Doineau [a], Sasikumar Mayarambakam [b], Bruno Schmaltz [b], Guylaine Poulin-Vittrant [a],[*]

[a] GREMAN UMR 7347, Université de Tours, CNRS, INSA Centre Val de Loire, 37071 Tours, France
[b] PCM2E EA 6299, Université de Tours, Parc de Grandmont, 37200 Tours, France

A B S T R A C T

Due to their excellent properties, Zinc oxide nanowires (ZnO NW) have been attractive and considered as a promising electron-transporting layer (ETL) in flexible Perovskite Solar Cells (FPSCs). Since the first report on ZnO NWs-based FPSCs giving 2.6 % power conversion efficiency (in 2013), great improvements have been made, allowing to reach up to~15 % nowadays. However, some issues still need to be addressed, especially on flexible substrates, to achieve uniform and well-aligned ZnO NWs via low-cost chemical solution techniques. Several parameters, such as the growing method (time, temperature, precursors concentration), addition of seed layer (thickness, roughness, annealing temperature) and substrate (rigid or flexible), play a crucial role in ZnO NWs properties (i.e., length, diameter, density and aspect ratio). In this review, these parameters allowing to control the properties of ZnO NWs, like the growth techniques, utilization of seed layers and the growing method (time or precursors concentration) have been summarized. Then, a particular focus on the ZnO NW's role in FPSCs as well as the use of these results on the development of ZnO NWs-based FPSCs have been highlighted.

1. Introduction

Zinc oxide (ZnO) is one of the most versatile semiconducting materials (II-VI binary compound group). The micro and nanostructures, especially ZnO nanowires (NW), have attracted massive interest and are beneficial for day-to-day life practical applications like photovoltaics (PV) [1], piezoelectric nanogenerators (PENG) [2], gas or bio-sensors [3,4], supercapacitors [5], light emitting diodes (LED) [6], etc., due to their promising properties, such as broader bandgap (3.37 eV) [7], higher electron mobility (200–300 cm^2/Vs) [8], higher exciton binding energy (60 meV) [9], and excellent conductivity [10]. The electron-transporting layer (ETL) is one of the key elements in Perovskite Solar Cells (PSCs). Usually, the ETL is sandwiched between the light-harvesting absorber and the top electrode (such as FTO & ITO) to extract the electrons efficiently and block holes. Recently, ZnO NWs have been highlighted as a potential alternative ETL in PSCs replacing conventional TiO$_2$ for the following reasons: (1) higher electron mobility [11], (2) easy processability from solution at low temperature, (3) vertically aligned NWs deliver a suitable direction for charge transfer (i.e., e$^-$) due to absence of grain boundaries, (4) better control of the NW length, diameter, density which can facilitate the absorber layer deposition

over the ETL. Apart from conventional TiO_2 and at the same time compared to widely used SnO_2, the ZnO ETL offers excellent electron mobility, which supports fast electron transport in PSCs. For example, Ruiqin He et al. calculated the e^- mobility using the SCLC method (i.e., space charge limited current), confirming that the ZnO ETL demonstrate higher electron mobility than SnO_2 and ZnO–SnO_2 ETLs [12]. In addition, ZnO provides better energy level alignment with the transparent electrodes (i.e., ITO and FTO) than SnO_2 ETL, and it smooths a surface. Due to that, ZnO is also used as an anode modification layer to enhance the efficiency in SnO_2 ETL-based PSCs [13–15]. However, the proton-transfer reaction between the ZnO-ETL/perovskite interface, specifically using volatile Methylammonium (MA) mixed perovskite composition, leads to poor device performance and stability [16,17]. In addition, several reports confirm that avoiding or having a minimum amount of MA cation in perovskite compositions greatly enhances the stability of the ZnO/perovskite interface [18–20].

Furthermore, flexible devices have gained tremendous attention because of their interesting properties: in addition to their flexibility, they are light-weight and easily reshapable. Wide applications such as flexible solar cells (house or industrial roofing, solar backpack), electronic textiles (wearable solar clothing), portable electric chargers and power sources for electric vehicles stand out from rigid substrates-based devices. Nevertheless, more issues come with the choice of substrate. For example, flexible PSCs (FPSCs), especially those using TiO_2 ETL, usually deposited by solution-processed spray pyrolysis or spin coating techniques in most cases [21, 22], require high temperature (>450 °C) treatment, degrading the substrate. However, amorphous-TiO_2 ETL fabricated by DC magnetron sputtering at usual room temperature (RT) [23], hydrothermal synthesis of TiO_2 nanoparticles (at 180 °C) and deposited at RT [24], and PE-ALD deposition of TiO_2 at 80 °C [25,26], are reported so far for FPSCs. Indeed, flexible plastic substrates, such as polyethylene terephthalate (simply - PET) or poly (ethylene 2,6-naphthalate) (i.e., PEN), are not stable at high temperatures compared to FTO or ITO-based rigid substrates [27]. Moreover, planar (*n-i-p* or front electrode/ETL/absorber/HTL/back electrode) or inverted (*p-i-n* or front electrode/HTL/absorber/ETL/back electrode) device architectures [28–30] are adopted while fabricating FPSC rather than the mesostructures [31]. Because mesoporous device architecture generally consists of mesoporous TiO_2, with a large number of pores residing in the bottom of the perovskite absorber that facilitates electron extraction. However, preparing mesoporous TiO_2, especially using the higher sintering process, is limited for flexible device fabrication due to the temperature limit of flexible substrates.

In the literature, many synthesis techniques are used for ZnO NW growth, such as hydrothermal deposition, vapor-liquid-solid process, flame transport approach and pulsed laser ablation [32]. Our group published several papers where the hydrothermal deposition method lead to well-aligned ZnO NWs for PSCs [33] and flexible PENGs [2,34,35], using different seed layers. Therefore, this review will focus on the limitations of the hydrothermal growth parameters to achieve optimal ZnO NWs for FPSCs and the impact of the seed layer on the latter ZnO NWs. It is worth mentioning here that very few reviews have been focused on ZnO NWs for solar cells

Fig. 1. Schematic of ZnO crystal structures: (a) CRS, (b) cubic ZB, and (c) HW. (d) Various crystal planes of hexagonal würtzite structure and (e) 3D view of hexagonal würtzite unit cell. Adapted from Ref. [37]. Copyright 2023 Elsevier.

[1,10,36]. To stand out from these published reviews, this one pays attention to flexible substrates-based PSCs compared to rigid substrates-based PSCs.

2. Properties and synthesis of ZnO nanowires

After a brief reminder of the ZnO nanowires crystalline structure (sec 2.1) and the possible synthesis methods (sec 2.2), the review will focus on hydrothermal synthesis of ZnO NWs. In particular, we will present how and why the ZnO NWs morphological properties (length, diameter and surface density) are influenced by the seed layer properties (sec 2.3), the growing time (sec 2.4) and finally, the chemical precursor concentrations (sec 2.5).

2.1. Crystalline structure

Usually, ZnO offers three crystal structures, namely (1) cubic rocksalt, (2) cubic zinc blende, and (3) hexagonal würtzite and noticeably each cation (Zn^{2+}) is encircled by four anions (O^{2-}) atoms at the vertices of a tetrahedron, and vice versa, which is corresponding to the covalent sp^3 bond (Fig. 1a–c) [37]. Among these structures, hexagonal würtzite (named HW–ZnO) is the most thermodynamically favoured and stable structure at normal ambient conditions. Nevertheless, the zinc blende (ZB) structure can be stabilized while growing on cubic substrates, and the cubic rocksalt (CRS) structure can be obtained at high pressure (over 9.5 GPa [8, 38]).

The HW–ZnO structure is adopting $P6_3mc$ or C_{6v}^4 space group with lattice parameter values of a = 3.249 Å & c = 5.207 Å, is composed of two interpenetrating hexagonal-close-packed (hcp) sub-lattices (i.e., hexagonal lattice of Zn^{2+} & O^{2-}), respectively [39]. The polarity of the surface, created by Zn^{2+} and O^{2-} atoms along the hexagonal plane (c-axis), is a reason for the ZnO crystal growth and the different nanostructures morphologies (nanorods and nanowires). Fig. 1d and e shows, respectively, the existing crystal planes and the 3D unit cell view of the HW structure. The HW–ZnO structure has two polar (i,e., [0001] terminated by Zn^{2+} and [000$\bar{1}$] terminated by O^{2-}, along the c-axis) and two nonpolar surfaces (i,e., [11$\bar{2}$0] and [10$\bar{1}$0] having an equal number of both atoms along the a-axis). Usually, the polar surfaces are also responsible for the piezoelectricity, defect generation and plasticity [37,40].

2.2. Growth techniques and seed layers for ZnO NW growth

The ZnO nanostructures employed in various fields and their applications need different requirements. For example, solar cells require smooth and well-aligned ZnO NWs with an appropriate NW length and void fraction, offering an efficient electron transfer between the absorber and the top electrode [33]. For the ZnO NW synthesis, various physical and chemical methods have been considered, such as hydrothermal growth (HTG) and/or chemical bath deposition (CBD) [33,34,41–43], vapor-liquid-solid process [44], flame transport approach [45], pulsed laser deposition [46], molecular beam epitaxy [47], electrospinning [48]. For further details on ZnO NW growth techniques, one should refer to published reviews [7,32,36,43,49]. However, most synthesis methods are restricted by utilization of high temperatures, which cannot be suitable for flexible substrates. In that consideration, the HTG process gives several benefits, for example, low material cost, easy & simple processing, environmentally friendly, and most importantly,
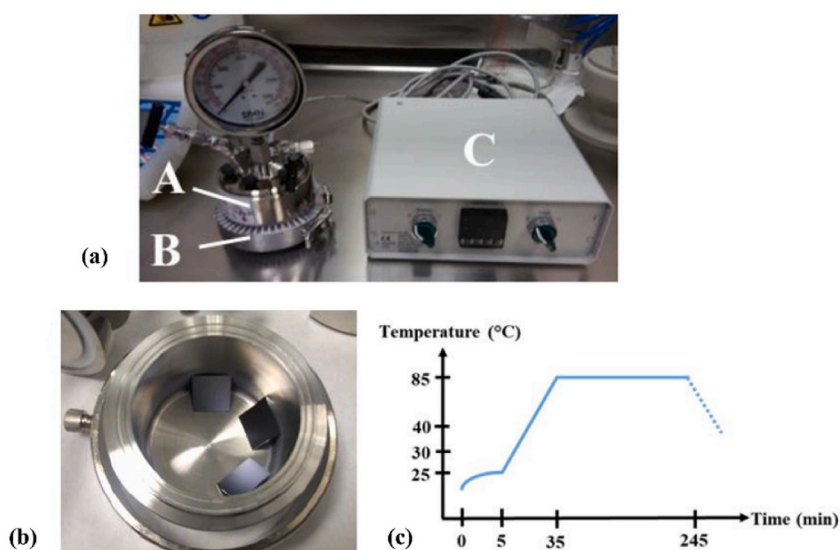

Fig. 2. Schematic representation of HTG process to grow high-quality ZnO NWs. Adapted from Ref. [34]. (a) A - Rustless steel autoclave, B - Heating ring, and C - Temperature controller. (b) Arrangement of samples inside the autoclave and (c) Temperature profile set.

low-temperature (less than 100 °C) process. Our team is consistently working on ZnO NW growth and has published several papers regarding ZnO NW growth for FETs (field-effect transistors), nanogenerators and Solar Cells using rigid and flexible substrates [2,34, 35,50–53]. The ZnO NW HTG growth set-up used in our group is shown in Fig. 2a–c, and the whole ZnO NW synthesis technique is thoroughly explained in our previous publication [34].

2.3. Influence of the seed layer on ZnO NW properties

The seed layer (for example, ZnO/Aluminum-doped zinc oxide (AZO)) is usually required to achieve a high-quality, well-aligned ZnO NW growth. The lattice mismatch is consequently reduced between the substrates and the ZnO NWs, which improves the length, the alignment as well as the homogeneity of the NWs [54,55]. In PSCs, the seed layer on flexible (PET/ITO) or rigid (FTO, ITO) substrate behaves as a hole (i.e., h^+) blocking layer that minimizes the recombination issues and thus improves efficiency. Moreover, the seed layer supplies nucleation centers (i.e., acts as seed spots), which consume Zn nutrients to produce ZnO NWs [56,57]. Previously published reports clearly explain that the annealing temperature (100 °C - 200 °C) and thickness of the seed layer directly influence the ZnO NWs properties such as the morphology, the growth orientation, the density, the diameter as well as the aspect ratio due to the changes in the seed layer surface roughness [34,57]. Moreover, to grow uniform ZnO NWs, the appropriate seed layer thickness and surface roughness are crucial. In general, several factors impact the film roughness, such as fabrication methods (i.e., spin-coating, RF sputtering, etc) and other conditions, such as annealing temperature, ultraviolet ozone (UVO) treatment, etc. For example, Matthew Kam et al. results demonstrate that the sputtered SnO_2 ETL film shows a lower surface roughness than spin-coated SnO_2 ETL film [58]. Andrzej Sławek et al. studies confirm that the precursor concentrations with different spin-coating speeds affect the film thickness and the surface roughness [59]. Ji-Sub Park et al. investigations show that the suitable annealing temperature with UVO treatment films offers a lower surface roughness than without UVO treatment films [56]. As a result, the fabrication techniques and other factors significantly affect the film properties, including surface roughness.

A summary of the ZnO seed layer surface roughness and the ZnO NWs properties (i.e., length, diameter & density) as a function of ZnO seed layer thickness, is shown in Fig. 3a–d. It is clear from Fig. 3a and **b** that the surface roughness and NW densities increased while NW length and diameters reduced with respect to the seed layer thickness. Also, it shows that a thicker seed layer offers higher surface roughness and reduces NW length. Moreover, L-W Ji et al. studies explain that a thinner seed layer with poor crystal characteristics produces poorly aligned NWs; meanwhile, thicker seed layers with good crystalline structure offer vertical well-aligned
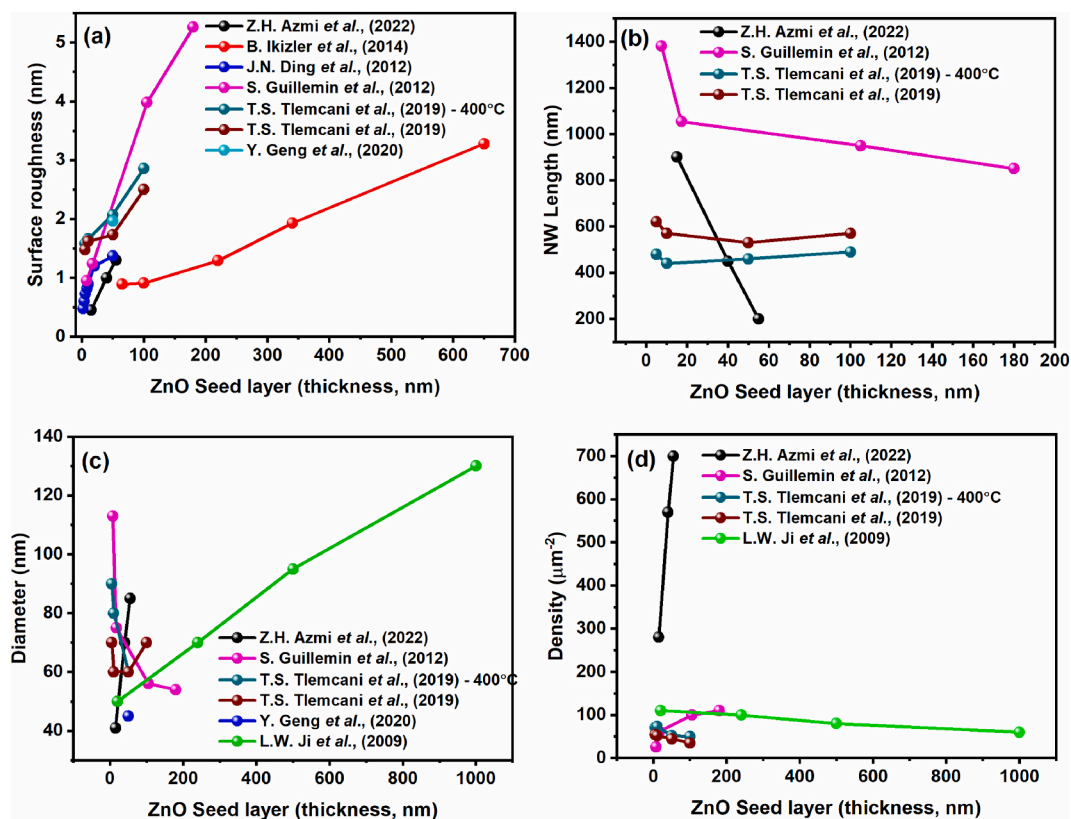
Fig. 3. ZnO seed layer properties (a) Surface roughness and (b) ZnO NWs Length, (c) ZnO NWs Diameter, and (d) ZnO NWs Density as a function of ZnO seed layer thickness [34,60,63–67].

uniform NW growth [60]. Also, Y. K. Abeykoon et al. reports explain that the decrement of the adhesive energy with the enhancing residual stress of the seed layer, especially while increasing seed layer thickness, possibly creates the detachment between the seed layer and the NWs [61]. Thermal annealing is a common method to influence the seed layer properties before ZnO NWs growth. For example, a low annealing temperature (80 °C [56]) leads to poor surface roughness, resulting in a lesser ZnO NWs density because of the smaller nucleation sites with limited coverage density and insufficient seed layer thickness (38 nm at 80 °C [56]). According to the published reports [56,57], higher annealing temperatures produced supplementary ZnO active nucleation sites in the seed layer, which may possibly enhance the thickness (56 nm at 180 °C). In parallel, high annealing temperature increases the seed molecule aggregations, increasing the seed layer's surface roughness [56,57]. The seed layer deposition settings, for example, deposition time, annealing temperature as well as precursor concentrations, effectively impact the ZnO NW properties [34,62]. Therefore, it is evident that in order to grow high-quality uniform ZnO NWs, optimizing the seed layer properties (thickness, surface roughness, including crystalline orientation and alignment) is essential, which indirectly depends on the chosen substrate. Moreover, the seed layer generally defines the adsorption of active nucleation sites.

2.4. Effect of growing time on ZnO NW properties

The NW growing time is a key parameter to adjust the morphology of the ZnO NWs: length, diameter, density as well as the distance between the NWs. The initiation and stimulation of the ZnO NWs growth require a minimum of 1.15 h (i.e., 75 min). A shorter time do not lead to a well-organized, dense and uniform NW array [68]. Fig. 4 summarizes the impact of the growing time on ZnO NWs properties: length, diameter as well as density. As we can see, the NW length and diameter are significantly increased with increasing growing time. Simultaneously, the NW density is reduced. As an example, H. Zhitao et al. show that a shorter growing time (2 h) leads to around 2 μm length NW without proper alignment. But a longer growing time (10 h) enhances the NW length to 25 μm, noticeably, with long and uniform NWs [69]. The lateral and the axial growth are concomitant during the early growth stage, which could affect the NW alignment more than the later growth stage. The decrease of the NW density can be explained by the faster axial direction NW growth compared to the lateral direction growth [69]. In some cases, after a specific growing time (6 h [67]), the NW length, diameter and density are saturated due to the unchanged overall Gibbs free energy (i.e., thermodynamic equilibrium state) and the lower NW growth rate. Therefore, it is understandable that achieving suitable NW properties depends not solely on the growing time but also on the chosen precursors concentration [67,70].

2.5. Effect of chemical precursors concentration on ZnO NW properties

Usually, the variation of the chemical reactant concentration affects the final products. The precursors concentration amount in the aqueous solution plays a vital role in the ZnO NW growth. Zinc nitrate hexahydrate, hexamethylenetetramine (HMTA), ammonium hydroxide, polyethylenimine branched (PEI), and ammonia are commonly used chemicals for the HTG - ZnO NWs growth [33,49]. Scheme 1 lists reactions that occur in the ZnO NW growth process [73,74]: decomposition reaction of HMTA (eq 1), hydroxyl supply reaction (eq 2), zinc nitrate reaction (eq 3) supersaturation reaction (eq 4 and 5) and ZnO NW growth reaction (eq 6 and 7) [73,74].

HMTA and $Zn(NO_3)_2$ are the primary contributors in the production of high-quality ZnO NW, the ammonia (NH_3) and OH^- mainly produced from HMTA (eq 1 and 2, Scheme 1), also play a role. The zinc nitrate hexahydrate yields zinc and nitrate ions and is also assumed to increase OH^- ion concentration. (eq 3 Scheme 1). The combination of OH^- and Zn^{2+} ions produces the intermediate of growth $Zn(OH)_2$. Simultaneously, Zn^{2+} ions combined with NH_4^+ yield to $Zn(NH_3)_4^{2+}$ (eq 4 and 5, Scheme 1). Finally, due to dehydration of the complex in the alkaline medium and the electrostatic attraction of Zn^{2+} and OH^- ionic species, ZnO clusters (NW) grow (eq 6 and 7, Scheme 1) [73]. Maintaining the appropriate saturation level in the precursors concentration during the ZnO NW growth is essential, which is generally achieved by controlling the OH^- concentration in the solution [75].

HMTA efficiently controls the ZnO NW growth direction because of its ability to attach the nonpolar facets of the NWs. Additionally, HMTA avoids attracting Zn^{2+} ion species, resulting in an only polar face epitaxial growth [75]. Fig. 5a and **b** presents the
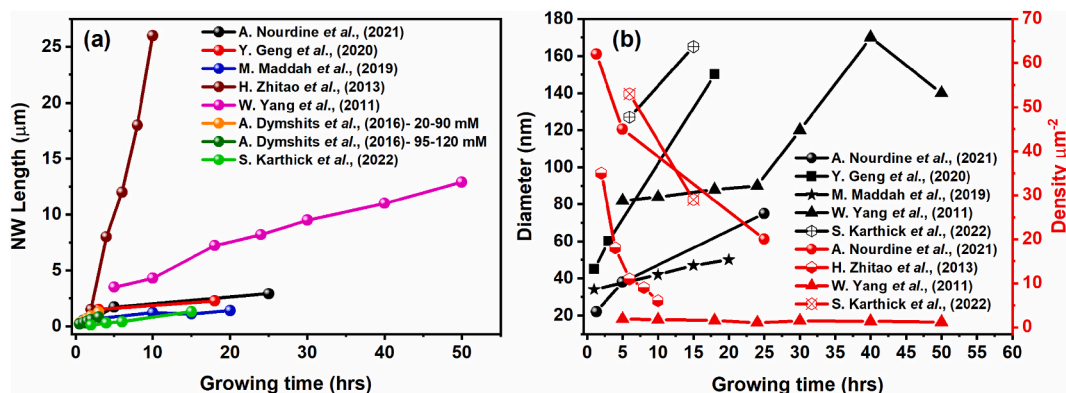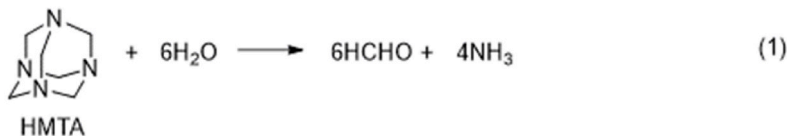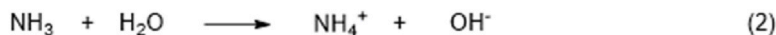

Fig. 4. ZnO NWs properties: (a) Length, (b) Diameter and Density with respect to the growing time [33,67–72].

Decomposition reaction of HMTA:
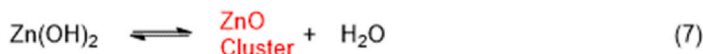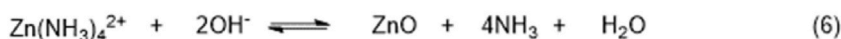
$$HMTA + 6H_2O \longrightarrow 6HCHO + 4NH_3 \tag{1}$$

Hydroxyl (OH^-) supply reaction:

$$NH_3 + H_2O \longrightarrow NH_4^+ + OH^- \tag{2}$$

Zinc nitrate reaction:

$$Zn(NO_3)_2 \longrightarrow Zn^{2+} + 2NO_3^- \tag{3}$$

Supersaturation reaction:

$$Zn^{2+} + 2OH^- \longrightarrow Zn(OH)_2 \tag{4}$$

$$Zn^{2+} + 4NH_3 \longrightarrow Zn(NH_3)_4^{2+} \tag{5}$$
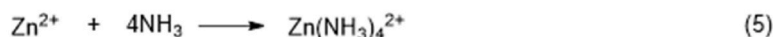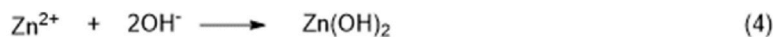
ZnO nanowire growth reaction:

$$Zn(NH_3)_4^{2+} + 2OH^- \rightleftharpoons ZnO + 4NH_3 + H_2O \tag{6}$$

$$Zn(OH)_2 \rightleftharpoons ZnO\ Cluster + H_2O \tag{7}$$

Scheme 1. Type of reactions occurs in the ZnO NW growth [73,74].

variation of the ZnO NWs length as well as diameter as a function of Zn – HMTA and PEI precursor's concentrations. Fig. 5a shows that the ZnO NW length and diameter are significantly increased with respect to the chosen Zn and HMTA concentration range. Indeed, more nucleation points can be originated when the precursor concentration is increased. On the opposite, less nucleation points are generated due to limited chemical reagents at the lower concentration [67]. Then, the NW growth rate increases faster along the c-axis compared to the lateral direction, resulting in NWs aspect ratio increment (for example, 5 for 2.5 mM and 36 for 15 mM [70]). After a Zn and HMTA concentration of 15 mM, the NW growth rate along the c-axis touches a quasi-saturation point, which means the diffusion as well as the reaction rate equalized, reducing the NW aspect ratio (20 for 50 mM, Fig. 4b in Ref. [70]). After this value (15 mM), the NWs start growing faster in the lateral direction. At one point, the lateral growth also meets a quasi-saturation point (at 50
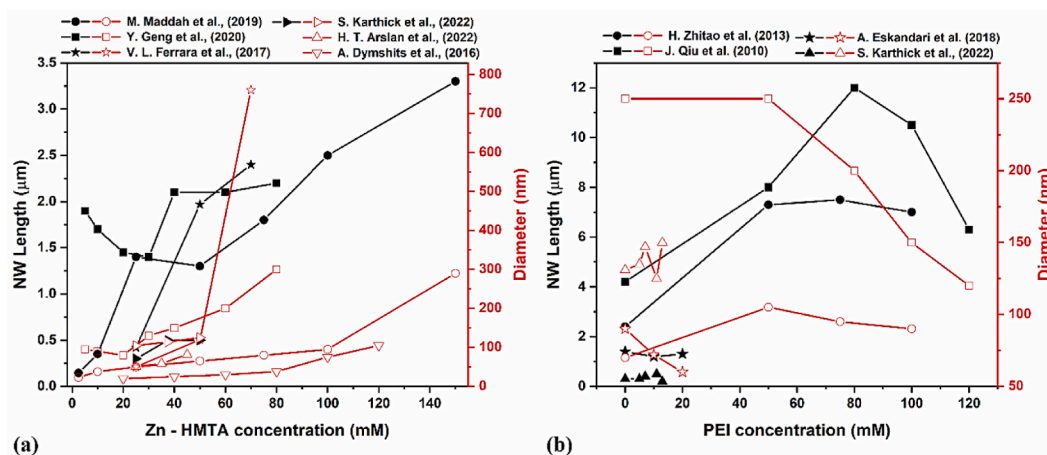
Fig. 5. ZnO NWs properties: Length and Diameter as a function of a) Zn-HMTA and b) PEI concentrations [33,67,69–71,77–80].

mM), and the NWs growth continues in both directions uniformly [70]. The Zn and HMTA concentration is very high (150 mM), which allows the new ZnO NWs to nucleate over the bottom NWs surface [70]. However, space as well as mass transport still reduce further crystal growth [67,76].

Noticeably, in the initial stage, due to heat, HMTA forms NH_3 and formaldehyde (HCHO), and HCHO is not directly involved in the NWs growth [33,81,82]. Therefore, adding PEI into the NW growth solution slowly reacts with HCHO, producing imine bonds. The reason comes from the fact that PEI consists of three kinds of amine groups, which include the primary (-NH_2), secondary (–NH–), and tertiary amines. Among these, –NH_2 & –NH– groups having the activated H atoms can react with HCHO, forming –N=CH- & –N=CH$_2$ groups [82]. So, the precursor solution turns yellow [79,82]. In PEI containing NW solution, 6 reaction steps are occurring, as shown in Scheme 2 [79,82]. The reactions are as follows: (1) decomposition of HMTA in ammonia and formaldehyde, (2) the chelation between PEI and Zn^{2+} ions, (3) the Mannich reaction, (4) the protonation of amine groups from PEI, (5 & 6), formation of $Zn(OH)_4^{2-}$ or Zn $(NH_3)_4(OH)_2$ followed by dehydration to start NW growth.

Fig. 5b illustrates the impact of PEI concentration on NWs length as well as diameter. It shows that the NW length and diameters increase to an optimum. Then, both NW length and diameters are reduced according to the PEI concentration [69,79]. The addition of PEI supports the NW growth alongside the polar c-axis and restricting the sidewall expansion, inducing the vertical alignment. Moreover, the PEI molecular weights and the PEI concentration modify the pH of the mixture, which directly influences the super-saturation level, resulting in different NWs lengths [83]. It is important to mention here that the value of the pH is also essential in the ZnO NW growth because the pH of the chosen precursor solution is not completely neutral; generally, the OH^- ions always exist in the solution. Additionally, the pH of the precursor solution changes due to the addition of alkaline reagents, applied temperature and growing time, resulting in differences in morphological behavior [84]. The density of the NWs reduces due to the availability of a lower pH value in the precursor's solution, forming an acidic environment which possibly etches the seed layer, and no ZnO NW growth is obtained at a lower pH range (pH < 4.6 [85] and pH = 2.8 [86]) due to the absence of Zn complexes. Therefore, precursor's concentration, temperature and growing time significantly influence the NWs properties, and the NWs length, density, diameter and aspect ratio can be controlled based on the requirement or applications.

3. ZnO NW's role in flexible perovskite solar cells (FPSCs)

Recently, flexible substrates-based Perovskite Solar Cells have reached a power conversion efficiency of over 22 % [87]. However, the PV performances are still below the rigid substrate-based devices, mostly due to (1) lower transmittance, (2) temperature tolerance as well as the thermal conductivity of flexible substrates, meaning the superiority of the perovskite absorber layer to the annealing process, and (3) the difficulty to control the absorbing layer morphology/surface [21,28,29,88]. Nevertheless, using roll-to-roll (R2R) printing technology eases the large-scale production of FPSCs, which opens the door for commercialization. Several published papers effectively explain the importance of the device architecture and the choice of the perovskite composition/mixture, and the ETL, HTL as well as top/bottom electrodes [28–30]. The choice of ETL and HTL materials (generally defines the energy level alignment between the layers) and the appropriate device architecture are crucial to improving the FPSC performances. Noticeably, high-performance flexible PSCs require high optical transmittance-based flexible substrates. Table 1 indicates the transmittance of common flexible substrates. These substrates are coated with TCO (transparent conducting oxides, for example, FTO & ITO) with excellent electrical conductivity, which generally determines the amount of photons that will reach the absorber layer as well as the charge transfer. The commonly used flexible substrates are PET, PEN, CPI (colorless polyimide), PS (polystyrene), polyimide (PI), PC (polycarbonate), PES
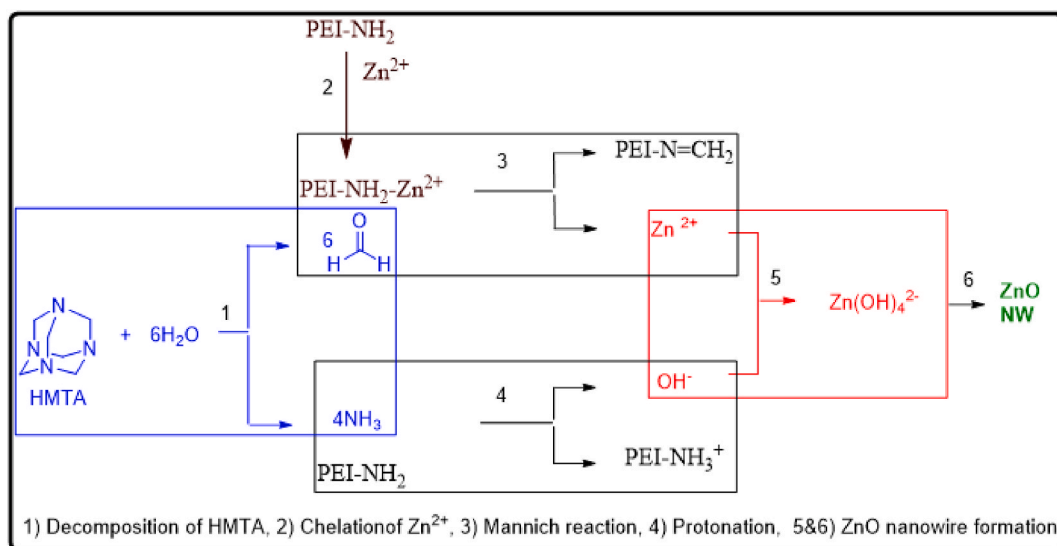
Scheme 2. Types of reactions occurring with PEI during ZnO NW hydrothermal growth [79,82].

Table 1
Summarized basic parameters for flexible substrates [27–29,88–98].

Substrate	T (%)	T_g (°C)	CTE (ppm/°C)	Modulus (Gpa)	Density (g/cm^3)	WA (%)	WVTR (g/cm^2/day)
PET	92	150	15–33	2–4.1	1.39	0.4–0.6	21
PEN	87	180	20	0.1–0.5	1.36	0.2	6.9
PES	88	223	214	–	1.37	0.43	73
PC	>89	150	75	2–2.6	1.20–1.22	0.4	60
PI	49	400	8–20	2.5	1.36–1.43	1.3–3.0	64
CPI	88	>350	29.2	2.8–4.5	1.23	2.1	93
FG	>90	700	2.5 ppm/°C	–	–	–	–
Nano-P	90	300	12–28.5	7.4–14	0.64	–	–
chNF-P	92	150	17.5	4.3	1.43	–	–
Mica	>90	600	1 ppm/°C	–	–	–	–

T – Transmittance, T_g – glass-transition temperature, CTE - coefficient of thermal expansion, WA -water absorption, WVTR – water-vapor transmission rate, CPI - Colourless PI, FG - Flexible glass, Nano-P - Nano paper, chNF-P - chNF paper.

(Polyether sulfone), etc. Table 1 summarizes the physical, chemical, and mechanical parameters of some common flexible substrates.

The thermal sensitivities of polymers restrict the TCO deposition on polymer substrates such as PEN or PET (Table 1). Usually, ITO is used as TCO on polymer flexible substrates rather than FTO. Indeed, ITO can be prepared at normal ambient temperature, whereas the deposition process for FTO is made at a high temperature (~350 °C), which is not suitable for polymer substrates [30]. V. Zardetto et al. extensively studied the electrical, optical, solvent resistance and elastic properties using several flexible substrates such as PET, PEN, ITO-coated PET and ITO-coated PEN compared with ITO and FTO-coated Glass [27]. These results clearly demonstrate that the sheet resistance values (i.e., electrical stability) remain stable (15 Ω/Sq) up to an optimum temperature (for example, PET/ITO~150 °C and PEN/ITO ~235 °C). Higher temperature significantly increases the sheet resistance by almost 20-fold for both substrates due to partial melting of ITO-coated PET and PEN. Consequently, high temperature severely affects the sample
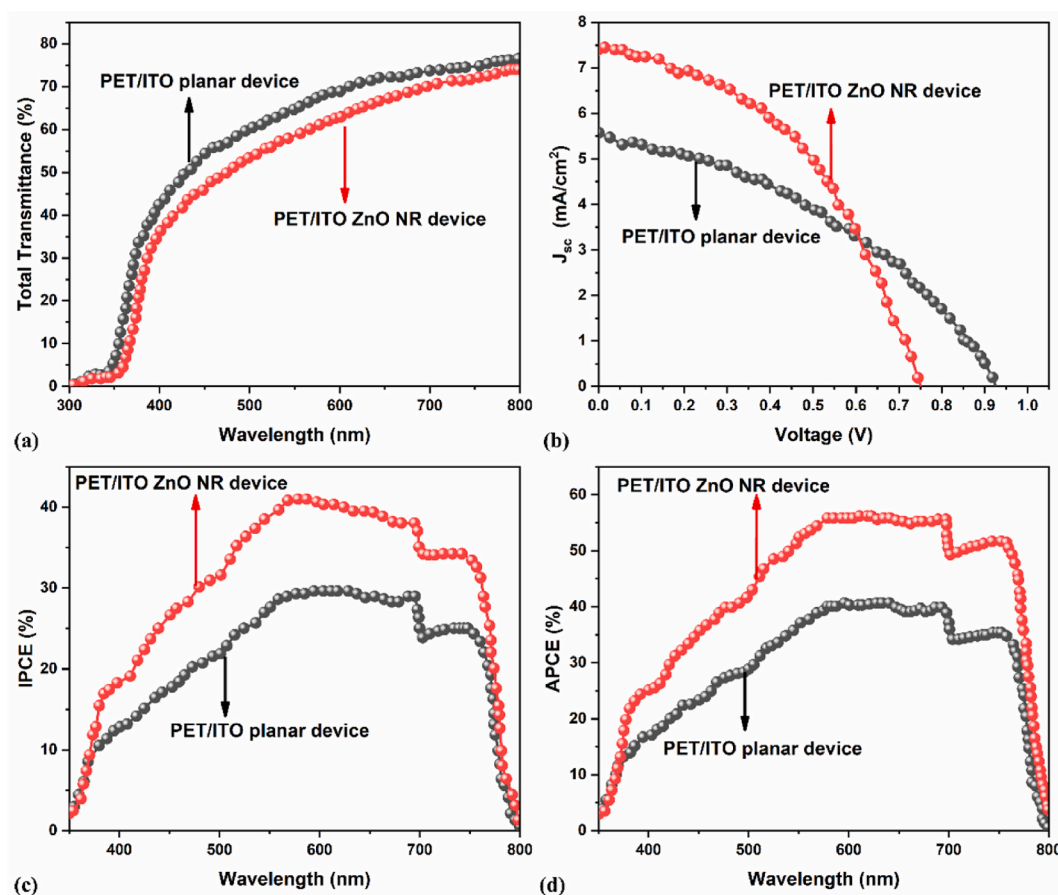

Fig. 6. (a) Total transmittance spectra, (b) current density Vs. Voltage plot, (c) IPCE spectra, as well as (d) APCE spectra for both planar and ZnO NR devices [100].

physical/shape formation. For example, PET/ITO films at 220 °C are completely rolled and almost melted at 250 °C (see Fig. 2b in Ref. [27]). Furthermore, their outcomes show that the PET substrate (with and without ITO) displays more optical transmittance spectra than PEN (with and without ITO). Commercially available PET/ITO substrates are mostly used in the flexible PSCs, especially in the lab scale devices. Many publications have shown over~20 % efficiency using PET/ITO substrate [21]. In addition, some review papers are dealing with the latest advancement, progress/growth and commercialization issues in the area of flexible PSCs [30,87,88, 92,99]. Interestingly, according to our knowledge, not a single review paper has been dedicated to the flexible PSCs employing ZnO NWs. Therefore, the following discussions will completely focus on the flexible PSCs using ZnO NWs in the perovskite device configuration.

In 2013, M. H. Kumar et al. reported the first FPSCs using ZnO nanorods (NRs)/ZnO seed layer with a PET/ITO substrate (60 Ω/sq), showing a PCE of 2.62 %. The efficiency is higher than for the planar flexible device (i.e., 2.18 %, without nanorods) adopting a lesser-temperature CBD process to grow the ZnO NRs (growth condition: 90 °C, and 90 min growing time) [100]. Fig. 6a–d shows the transmittance and PV characteristics (J-V), including the IPCE (incident photon to current efficiency) as well as APCE (absorbed photon-to-current conversion efficiency) performance of both planar and ZnO NR-containing flexible devices.

The results show that the obtained J_{sc} (i.e., current density) is considerably enhanced from 5.5 mA/cm^2 (without ZnO NRs) to 7.5 mA/cm^2 (with ZnO NRs) due to better charge collection and improved heterojunction interface compared to a conventional device. Noticeably, the ZnO nanorod-containing device shows a reduced V_{oc} (open-circuit voltage 0.80 V) compared to the standard device (i. e., 0.99 V). The authors attributed it to a higher recombination issue that possibly occurred due to the larger interfacial area.

In 2016, A. Dymshits et al. systematically investigated the factors manipulating the growth of ZnO NWs by adopting a low-temperature process to fabricate the FPSCs [71]. They employed ZnAc (i.e., zinc acetate dehydrate) as a seed layer to grow the ZnO NW by hydrothermal growth method (growth condition: 90 mM, 90 °C, and 90 min growing time) using both rigid (FTO-coated Glass) and flexible substrates (ITO-coated PET). Fig. 7a and **b** shows the J-V, internal quantum efficiency (IQE), and SEM cross-section image of ITO-coated PET/ZnAc/ZnO NW/MAPbI$_3$/Spiro-OMeTAD-HTL/Au FPSC, respectively. The results display that the rigid device offers higher efficiency (i.e., 9.06 %) than the flexible device (i.e., 6.39 %), and the SEM cross-section image of the FPSC device shows the penetration of the MAPbI$_3$ through the ZnO NW layer. The FPSC demonstrated good stability performance (using 75 bending cycles), noticeably less than 20 % of its initial value dropped after 35 cycles.

In 2016 [101] and 2019 [102], Zhong Lin Wang's group published an article focusing on the new approach named Piezo-phototronic effect (PPE) to enhance FPSCs performance using ZnO nanowire/microwire (NW/MW) on the flexible substrate. In their study, the ZnO seed layer was added by RF sputtering, and the lesser-temperature solution method was employed to grow ZnO NWs (growth condition: Zn(NO$_3$)$_2$ and HMTA (60 mmol/l), 85 °C and 90 min growing time). Fig. 8a–e shows the SEM top-view image ZnO NWs (avg diameter 200 nm), BF-TEM (bright field transmission electron microscopy) including the corresponding SAED (selected area electron diffraction) pattern, high-resolution TEM (HRTEM), and SEM cross-section image of ITO-coated PET/ZnO/ZnO NW/MAPbI$_3$/Spiro-OMeTAD-HTL/Au FPSC, respectively. The fabricated FPSC (i.e., non-strain device, see Fig. 9a–c) delivers 9.3 % efficiency with the solar cell parameters of J_{sc} = 17.8 mA/cm^2, V_{oc} = 0.89 V, and FF = 56 %, which is already higher than previously published FPSC reports (see Table 2) [71,100]. Later, they bent the FPSC device upward according to the device structure, and the ZnO nanowires experienced tensile strain, specifically in the NW growth direction (see Fig. 9d). On the other side, the ZnO nanowires experienced compressive strain while bending the FPSC device on the opposite side (i.e., downward, see Fig. 9g). Generally, the introduction of external strain, either tensile or compressive, modifies the ZnO NW/perovskite interface energy level by piezoelectric potential (positive or negative [103]). While applying external static tensile strains (i.e., 0.75 %, 1.06 %, 1.31 %, 1.52 %, 1.71 % and 1.88 %), the PV parameters are highly enhanced, especially the J_{sc} (see Fig. 10), which improves the PCE from 9.3 % to 12.8 % for 1.88 % strain value.

Fig. 9e shows that the tensile strain produced positive piezoelectric potential, reducing the charge transfer barrier height (see Fig. 9f) and facilitating the electron passage from the MAPbI$_3$ to ZnO NWs. On the contrary, when applying external static compressive
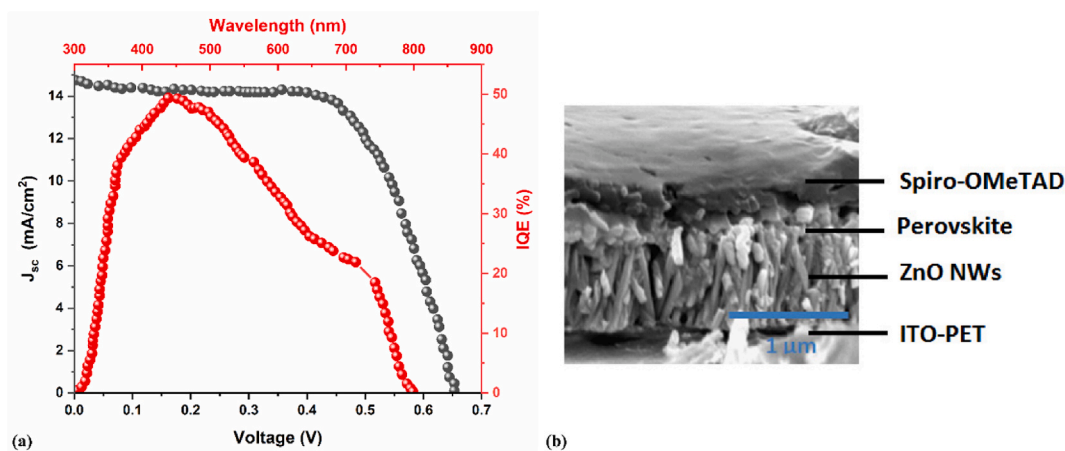

Fig. 7. (a) Current density Vs. Voltage and IQE graph (b) SEM cross-section of the FPSCs. Adapted from Ref. [71].
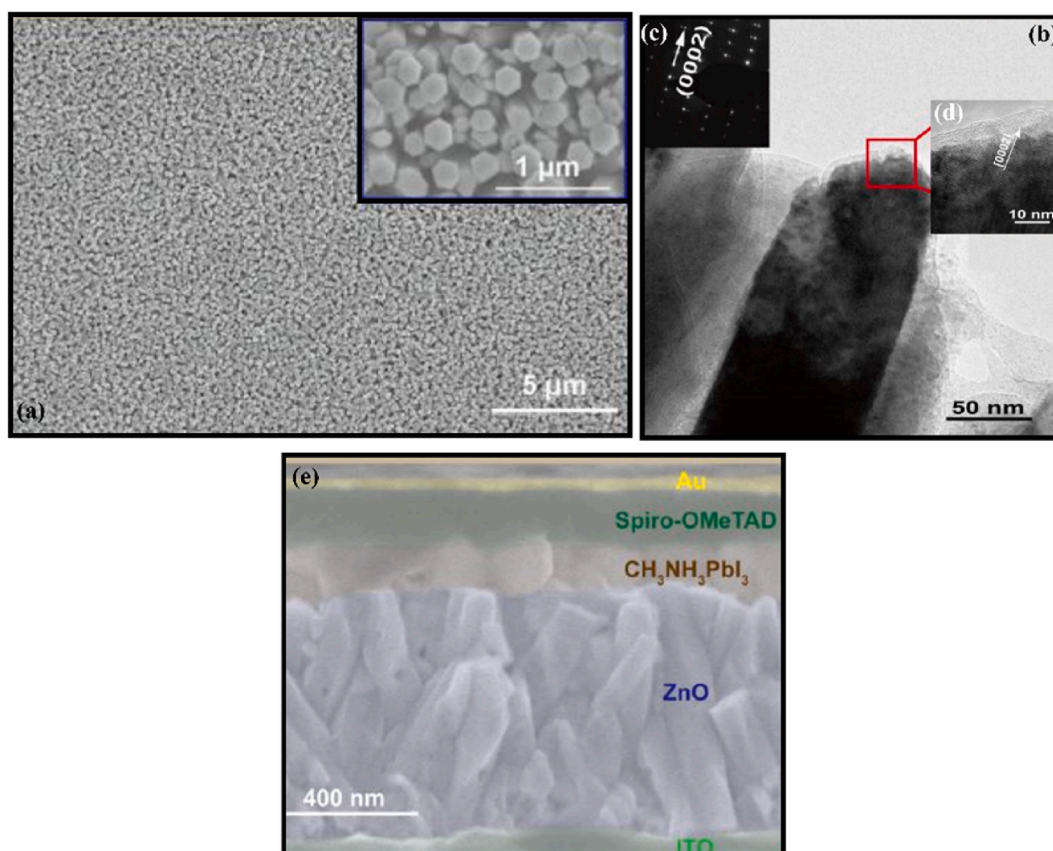
Fig. 8. (a) SEM top-view image of ZnO NWs (inset: the enlarged image), (b) BF-TEM image, (c) SAED pattern of the ZnO nanowires, (d) HRTEM image, and (e) SEM cross-section of the FPSCs. Reproduced from Ref. [102]. Copyright 2023 American Chemical Society.

strains (i.e., −0.75 %, −1.06 %, −1.31 %, and −1.52 %), the device performance was reduced from 9.3 % to 7.7 % (for a −1.52 % strain range) due to the current density reduction (see Fig. 10). In this instance, the negative piezoelectric potential induced at the perovskite/ZnO NW-ETL interface (see Fig. 9h), increasing charge barrier height (see Fig. 9i), affects the FPSC performance.

In 2020 F. Bouhjar et al. grew the cobalt–doped zinc oxide NWs (i.e., Co–ZnO NWs) using a hydrothermal process on PET/ITO substrate (growth conditions: (i) 150 °C, 4 h and (ii) 90 °C, 5 h to develop Co–ZnO nanostructures) [104]. The fabricated FPSC with the PET/ITO/Co–ZnO NR/MAPbI$_3$/Spiro-OMeTAD/Au device architecture offers an efficiency of 7 % (V_{oc} = 1.04 V, J_{sc} = 14.3 mA/cm^2, and FF = 47 %), and the corresponding J-V and IPCE graphs displayed in Fig. 11. The XRD (X-ray diffraction) result shows that the primary 002 plane peak (i.e., 2θ = 34.3°) is highly enhanced for PET/ITO/Co–ZnO NR compared to PET/ITO/ZnO film, which significantly indicates the crystallinity improvement. Their SEM image reveals that the diameters of Co–ZnO NRs are larger than un-doped ZnO NRs, and also, the Co–ZnO NRs film exhibits enhanced transmittance behavior in the visible region compared to ZnO NRs, which brings extra photons to the absorber.

The photo-current transient response of PET/ITO/Co–ZnO NRs and un-doped PET/ITO/ZnO NRs electrodes shows that the doped one displayed a 4-fold higher photo-current density (6 mA/cm^2). The Co-doping efficiently eases the charge carrier partition before recombination due to donor concentration enhancement compared to the un-doped case. The electrochemical impedance spectroscopy (EIS) results reveal that the Co–ZnO NRs sample shows lower series resistance (4.8 kΩ) compared to the pure sample (7.9 kΩ), which indicates the improvement in the charge transfer and reduction of the recombinations.

In 2021, M. Fahim et al. grew ZnO NRs and core-shell ZnO@ZnS NRs on flexible substrates (PET/ITO) using a hydrothermal method (growth condition: 90 °C and 3 h growing time) [19]. The newly added ZnS interlayer between ZnO NRs/perovskite interface modifies the energy level alignment, and it creates a robust Zn–S–Pb coordination bond with absorber (i.e., perovskite), easing the e$^-$ transport. Usually, the primary terminal surface hydroxyl group (−OH) on the ZnO surface induces the deprotonation (i.e., protons removal) of organic amine in perovskite, triggering the degradation of Perovskite Solar Cells [16,105]. Therefore, adding a ZnS interlayer improves the device stability due to the reduction of the –OH group on the ZnO surface.

The comparison of both surface and cross-sectional FE-SEM (field emission electron microscopy) images of ZnO NRs, as well as core-shell ZnO@ZnS NRs, is shown in Fig. 12a–f. It shows that during sulfidation (0.5 h), the ZnO surface is entirely etched, and ZnS growth creates an outline shell layer on the ZnO core (i.e., the ZnO surface is completely coated with a fine layer of ZnS, see Fig. 12d–f). The SEM and AFM images (Fig. 4c and Fig. S5 in Ref. [19]) demonstrate that the modified film (with ZnS) shows a compact and
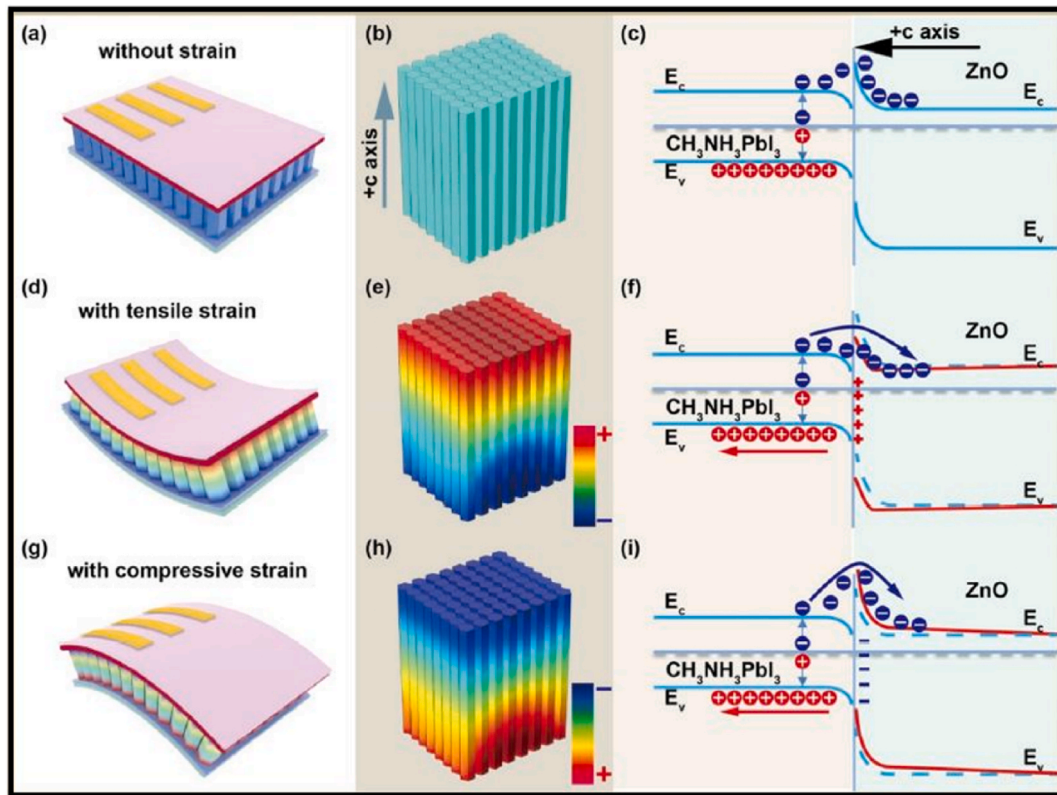
Fig. 9. (a, d, and g) Schematics, (b, e, and h) Piezo-potential distributions, and (c, f, and i) energy-band diagrams explaining the PPE on the FPSCs with non-strain, tensile and compressive strain, respectively [101,102]. Adapted from Ref. [102]. Copyright 2023 American Chemical Society.

Table 2
Summarized PV parameters for FPSCs using ZnO NWs with the corresponding device architectures.

No	FPSC device architecture	J_{sc} (mA/cm^2)	V_{oc} (V)	FF (%)	PCE (%)	ref
1	PET/ITO/ZnO/ZnO NR/MAPbI$_3$/HTL/Au	7.52	0.80	43	2.6	[100]
2	PET/ITO/ZnAc/ZnO NW/MAPbI$_3$/HTL/Au	14.42	0.68	65	6.4	[71]
3	PS/Ag/ZnO MW/MAPbI$_3$/HTL/Ag	8.70	0.86	42	0.3	[101]
4	PET/ITO/ZnO/ZnO NW/MAPbI$_3$/HTL/Au	17.80	0.89	56	9.3	[102]
	With Tensile strain (1.88 %)	23.50	0.95	59	12.8	
	With compressive strain (−1.52 %)	16.10	0.89	56	7.7	
5	PET/ITO/Co:ZnO NR/MAPbI$_3$/HTL/Au	14.30	1.04	47	7.0	[104]
6	PET/ITO/ZnO/ZnO NR/Cs$_{0.05}$(FA$_{0.83}$MA$_{0.17}$)$_{0.95}$Pb(I$_{2.6}$Br$_{0.4}$)/HTL/Ag	21.40	0.89	58	11.97	[19]
	With Tensile strain (1.5 %)	24.10	0.91	63	13.86	
	With compressive strain (−2 %)	18.30	0.86	61	9.88	
	PET/ITO/ZnO/core-shell ZnO@ZnS NRs/Cs$_{0.05}$(FA$_{0.83}$MA$_{0.17}$)$_{0.95}$Pb(I$_{2.6}$Br$_{0.4}$)/HTL/Ag	21.82	0.94	63	12.94	
	With Tensile strain (1.5 %)	24.40	0.97	63	14.68	
	With compressive strain (−2 %)	18.50	0.93	62	10.69	

HTL – Spiro-OMeTAD.

pinholes-free layer with a lower roughness (Ra = 9.57 nm) compared to conventional ZnO NRs films (i.e., irregular morphology with a higher Ra = 11.1 nm).

The fabricated core-shell ZnO@ZnS NR FPSC (i.e., non-strained device) shows 12.94 % efficiency with J_{sc} (21.82 mA/cm^2), V_{oc} (0.94 V) and FF (63 %), respectively. Meanwhile, the conventional ZnO NR FPSC delivers 11.97 % efficiency (21.40 mA/cm^2 (J_{sc}), 0.89 V (V_{oc}), and 62 % (FF)). While applying external static tensile strains (1.5 %), the device efficiency is enhanced by up to 14.68 % (core-shell ZnO@ZnS NR device) and 13.86 % (conventional ZnO NR device). On the other side, when applying compressive strains (i. e., −2 %), the device performance is reduced from 11.97 % to 9.88 % (conventional ZnO NR device) and from 12.94 to 10.69 % (modified device) due to the current density drop. The corresponding current density Vs. Voltage characteristics for conventional ZnO NR and ZnS added NR FPSCs with non-strain, tensile strain (1.5 %) and compressive strain (−2 %), are shown in Fig. 13a and b. IPCE graph characteristics for standard and modified (with ZnS) FPSCs and the SEM cross-sectional image of ZnO@ZnS NR FPSC are
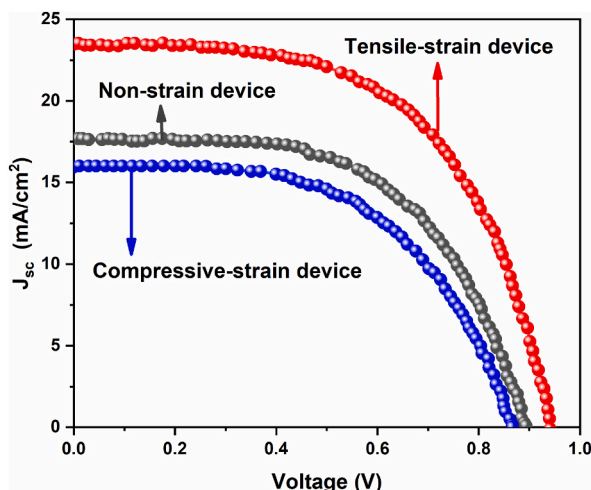
Fig. 10. J-V characteristics comparison of the FPSCs with non-strain, tensile strain (1.88 %) and compressive strain (−1.52 %), respectively [102].
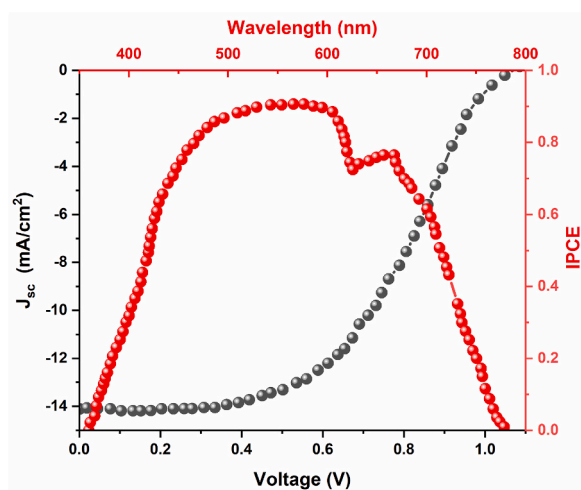

Fig. 11. Current density Vs. Voltage and IPCE graph characteristics of the FPSCs [104].

displayed in Fig. 13c and d. It shows the modified device (with ZnS) IPCE is more than 85 % in the visible region (i.e., permits more photons) compared to the conventional ZnO NR device. In the tensile strain case (1.5 %), the junction barrier height at interfaces (i.e., ZnS/ZnO as well as ZnS/perovskite) are modified due to piezoelectric potential (PEP) and the piezo polarization (PP) charges produced at both interfaces. That smooths the separation of the photoinduced charge carriers, as well as significantly suppresses the re-combinations, resulting in enhanced performance of both standard and modified (with ZnS) FPSCs. Indeed, the higher charge recombination issues occur in the compressive strain case (−2 %), reducing the device efficiencies. Therefore, using a core-shell structure (i.e., ZnO@ZnS NR) provides a promising path towards stable and excellent FPSC performance and will be highly benefi-cial for everyday applications such as wearable and compact electronic devices.

And only a few reports discussed the stability issues on ZnO NWs ETL-based FPSCs [19,71,100–102,104]. Importantly, M. Fahim et al. bending investigations confirm that the longstanding thermal and stability performance of modified (with ZnS) FPSCs is better than conventional ZnO NR FPSCs (Fig. 8 in Ref. [19]), which is mainly due to the minimized defects at ZnO/perovskite interface. Moreover, A. Dymshits et al. findings (i.e., 0 to 75 bending cycles with 1.2 cm radius bending, Fig. 5d in Ref. [71]) and J. Sun et al. results (i.e., 0 to 2000 bending cycles, Fig. S8 in Ref. [102]) evidently demonstrate that the long periods of bendings, either in the upward or downward direction, drastically reduce the FPSCs efficiency. The advancement of PV device efficiency using ZnO NWs on flexible substrates is shown in Fig. 14, and the corresponding device architectures and the PV parameters (PCE, J_{sc}, V_{oc}, and FF) are displayed in Table 2. It is worth mentioning here very few papers were available on ZnO NW/NR-based flexible perovskite solar cells. These data explain that the FPSCs PV performance with ZnO NW has been significantly enhanced in recent years from 2.6 % to up to~15 %. However, the ZnO NWs ETL flexible devices still displayed a lower PCE than other FPSCs. The possible reasons are sum-marized according to the published reports (1) higher recombinations at the interface (i.e., ZnO NWs/perovskite): and (2) the direct
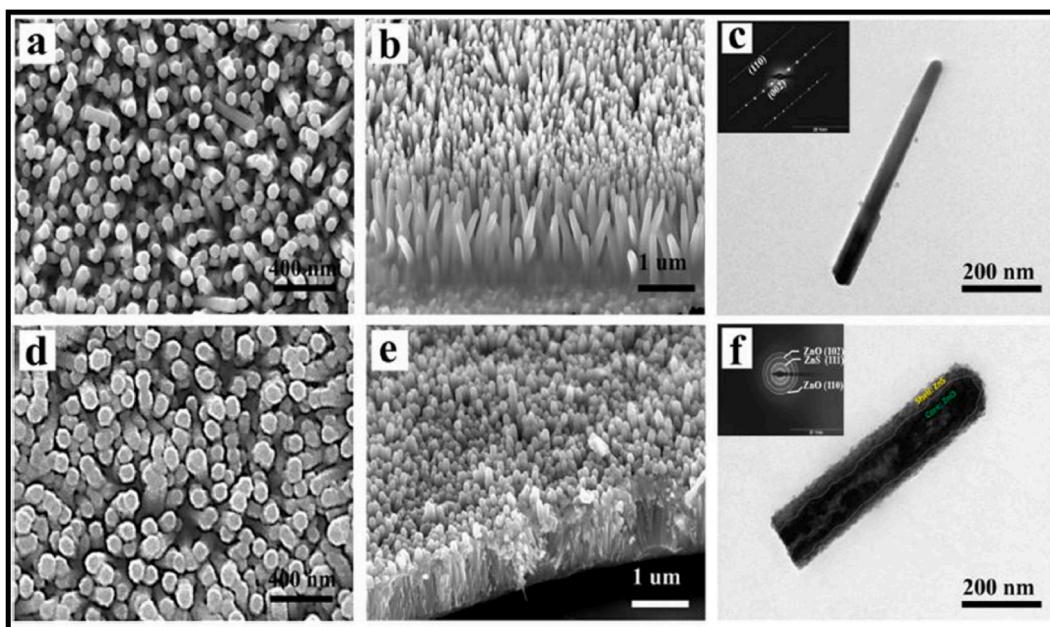
Fig. 12. SEM Surface and cross-sectional image comparison of (a, b) ZnO NRs and (d, e) core-shell ZnO@ZnS NRs. TEM image comparison of (c) ZnO NRs and (f) core-shell ZnO@ZnS NRs (inset shows the SAED patterns). Adapted from Ref. [19]. Copyright 2023 Elsevier.

connection between ZnO NWs-ETL into the HTL or, in simpler terms, penetration of NWs towards the HTL, which is due to higher NWs length or lower perovskite layer thickness, respectively [33,71,100–102,104]. It suggests that attaining a high efficiency using ZnO NWs, especially on flexible substrate-based PSC devices, is not easy compared to rigid substrate-based devices. Nevertheless, from a practical point of view, flexible devices have wider possible applications (i.e., compact electric chargers, microelectronic fabrics, enlarged industrial roofing, avionics, robotic insects and energy supplies for uncrewed aircrafts, etc.) and are more suitable than rigid devices [21,29,88,106,107].

Apart from the FPSCs, other flexible solar cells using ZnO NWs with the corresponding device architectures and PV parameters are shown in Table 3. In 2008, H. M. Unalan et al. investigated the flexible organic solar cell (F-OSC) employing ZnO NWs, and the fabricated device demonstrated an efficiency of~0.6 % [108]. In 2010, K. H. Lee et al. fabricated the flexible inverted organic SC (F-IOSC) using ZnO NRs on PES/ITO substrate, obtaining 0.98 % of PCE [109]. In 2011, S. Chu et al. studied ZnO NW arrays-based flexible dye-sensitized SC (F-DSSC) using PET/ITO, and it provides 0.44 % of efficiency, respectively [110]. In 2014, D. Y. Kim et al. fabricated the F-DSSC employing ZnO NRs, offering 0.69 % of PCE while using 18 h growth time with post-growth annealing treatment compared to 9 h growth sample (i.e., with and without post-annealing treatment) [111]. In 2016, Z. Li et al. fabricated the F-DSSC with ZnO NWs, and it delivered 1.78 % of PCE [112]. In the same year, M. K. Pathirane et al. examined the optical as well as electrical characteristics of hybrid SCs using ZnO NWs on the flexible substrate (PEN), and the corresponding device demonstrated an efficiency of 4 % [113]. Also, L. Zu et al. fabricated the ZnO NWs-based n-ZnO/P–SnS core-shell flexible SCs, and it show an efficiency of 1.2 % [114]. In 2017, Y. Wang et al. examined both rigid and flexible substrates (i.e., PET/ITO) based colloidal quantum dot SC (F-CQDSC) using ZnO NWs, exhibiting the PV performance of 4.35 %, it's lower than the rigid device efficiency (i.e., 5.35 %) [115]. The bending characteristics confirm that the ZnO NWs containing the F-CQDSC device retain 93 % of its initial efficiency (bending angle = 160°) compared to non-NW-based device performance. In 2018, S. Qiao et al. demonstrated the flexible CIGS solar cell with ZnO NWs, showing an efficiency of 4.82 %, and it enhances (i.e., 5.97 %) while applying −0.74 % of compressive strain, respectively [116]. Recently (in 2022), S. Pathania et al. studied the flexible polymer nanocomposites (PVK) based SC (F-PVKSC) performance adopting ZnO NRs with an ITO-coated PET/ZnO NRs/PVK/PEDOT:PSS/Ag SC configuration [117]. The ZnO NRs-containing device offers 2.07 % of PCE than the conventional one (i.e., without ZnO NRs, PCE = 1.38 %, J_{sc} = 7.47 mA/cm^2, V_{oc} = 0.43 V & FF = 43 %). Therefore, the combination of ZnO NWs-based FPSCs and other above-mentioned solar cells opens further new perspectives in the field of PV application, especially using flexible substrates.

4. Summary and perspectives

In this review, we demonstrated that ZnO NWs show a promising advantage for flexible devices. Physical properties and chemical preparation, including cost-effective methods, allow increasing the FPSC performance compared to the past few years. To grow ZnO NWs using a low-temperature HTG process, parameters mainly precursor's concentration, growing time, growth temperature as well as appropriate seed layer (ZnO or AZO) thickness, annealing temperature, and surface roughness need to be carefully controlled for flexible substrates, in order to achieve suitable ZnO NWs properties (such as NW length, NW diameter, NW density and aspect ratio).
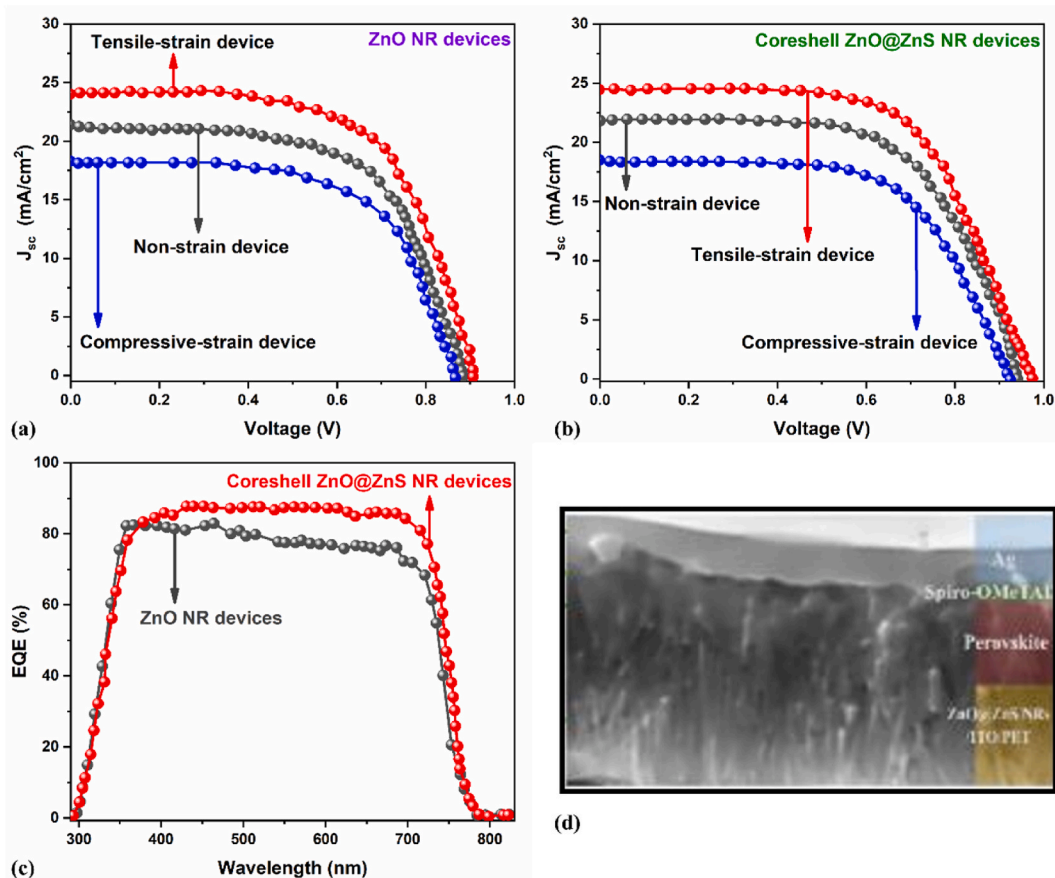
Fig. 13. Current density Vs. Voltage characteristics comparison of both (a) standard (with ZnO NR) and (b) modified (with ZnS) FPSCs with non-strain, tensile strain (1.5 %) and compressive strain (−2 %), respectively. (c) IPCE graph characteristics, and (d) SEM cross-sectional image of core-shell FPSC. Adapted from Ref. [19]. Copyright 2023 Elsevier.
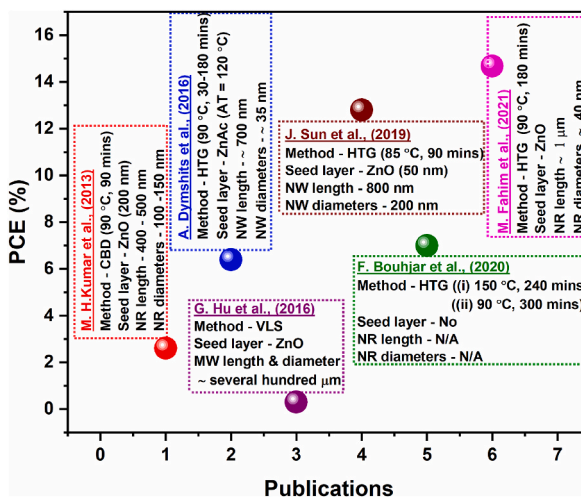

Fig. 14. PCE Vs. Publications of the flexible PSCs using ZnO NWs [71,100–102,104].. (Inset: ZnO NW/NR growing method and available NW/NR properties, CBD - Chemical bath deposition, HTG -Hydrothermal growth, VLS - Vapor-liquid-solid process.)

Table 3

Summarized PV parameters for other flexible solar cells using ZnO NWs with the corresponding device architectures.

No	FSC device architecture	J_{sc} (mA/cm^2)	V_{oc} (V)	FF (%)	PCE (%)	ref
1	PET/SWNT/ZnO NW/P3HT/Au	2.40	0.46		~0.60	[108]
2	PES/ITO/ZnO NW/P3HT:PCBM/MoOx/Au	9.92	0.26	37	0.98	[109]
3	PET/ITO/Pt/ZnO NW-based DSSC	2.73	0.40	40	0.44	[110]
4	PET/ITO/ZnO NR-based DSSC	3.95	0.65		0.69	[111]
5	Compacted stainless steel meshes-based F-DSSC	7.74	0.50	46	1.78	[112]
6	PEN/Cr/ZnO NW/a-Si:H/AZO/Ag	14.2	0.60	47	4.00	[113]
7	PET/ITO/ZnO NW/SnS/Ag	4.58	0.54	48	1.20	[114]
8	PET/ITO/ZnO NW/F-CQDSC/Au	18.15	0.51	47	4.35	[115]
9	ITO/ZnO NW/CdS/CIGS/Mo	18.81	0.50	51	4.82	[116]
	−0.74 % compressive strain	22.22	0.52	51	5.97	
10	PET/ITO/ZnO NRs/PVK/PEDOT:PSS/Ag	11.20	0.43	43	2.07	[117]

After discussing fundamental ZnO NWs properties and deposition methods, including the affecting parameters, we have discussed the crucial role of ZnO NWs in FPSCs. From the first device in 2013 (PCE = 2.6 %), FPSCs consisting of ZnO NW-based devices have since achieved promising efficiency, up to 15 %. However, the PCE of ZnO NWs-based flexible PSC and other flexible substrate-based such as DSCC, OSC, CQDSC, and other nanocomposites devices are still struggling to reach comparable performances with the rigid substrate-based ZnO NW devices, mainly due to the restrictions in device fabrication and material selection. Moreover, many papers do not provide complete information on the ZnO NWs properties (i.e., NW length, NW diameter, NW densities, as well as aspect ratio) or detailed synthesis conditions (for example, the etching method for ZnO NWs-ETL). Therefore, finding a trend, especially on the effect of NW properties on flexible PSCs performance, is more challenging.

After a careful investigation of the published reports (based on Fig. 14), HTG temperature and NWs length, respectively, between 85 °C and 90 °C and in the range of 500–1000 nm, is beneficial to achieve high-performance ZnO NWs-based FPSCs. However, some additional work is required to understand the trend in a better way: by studying further the impact of ZnO NWs properties on the FPSC performance (all other parameters fixed, like seed layer, absorber, HTL and electrodes); by investigating theoretical studies. Also, the following points are possibly beneficial for the successful device performance: (1) Optimizing ZnO NWs length smoothes the charge transfer from the absorber via optimizing thickness and annealing temperature, as well as the surface roughness of the seed layer. (2) Improving the flexible substrate/seed layer and/or seed layer/ZnO NWs interfaces, especially ZnO NWs/perovskite absorber via doping or interlayer (for example, Co-doped ZnO NR and core-shell ZnO@ZnS NRs), reducing the recombination and enhancing the charge transfer. In addition, it is worth mentioning that the optimization of the void fraction between the NWs will impact the perovskite infiltration and the quality of charge transfer. (3) Optimizing the perovskite absorber layer, such as perovskite composition (with multiple cation/anion) and layer thickness, including antisolvent treatment, additives, and thermal annealing. Finally, there are several challenges to improving the efficiency of flexible ZnO NWs-based PSCs. Therefore, more efforts are still needed to enhance the FPSCs performance further.

Data availability statement

All the discussed data are included in the manuscript.

CRediT authorship contribution statement

Karthick Sekar: Writing – review & editing, Writing – original draft, Investigation, Formal analysis, Conceptualization. **Raphaël Doineau:** Formal analysis. **Sasikumar Mayarambakam:** Formal analysis. **Bruno Schmaltz:** Writing – review & editing, Validation. **Guylaine Poulin-Vittrant:** Writing – review & editing, Validation, Supervision, Conceptualization.

Declaration of competing interest

The authors declare that they have no known competing financial interests or personal relationships that could have appeared to influence the work reported in this paper.

References

[1] V. Consonni, J. Briscoe, E. Kärber, X. Li, T. Cossuet, ZnO nanowires for solar cells: a comprehensive review, Nanotechnology 30 (2019) 362001, https://doi.org/10.1088/1361-6528/ab1f2e.

[2] T. Slimani Tlemcani, C. Justeau, K. Nadaud, D. Alquier, G. Poulin-vittrant, Fabrication of piezoelectric zno nanowires energy harvester on flexible substrate coated with various seed layer structures, Nanomaterials 11 (2021) 1433, https://doi.org/10.3390/nano11061433.

[3] D.P. Neveling, T.S. Van Den Heever, W.J. Perold, L.M.T. Dicks, A nanoforce ZnO nanowire-array biosensor for the detection and quantification of immunoglobulins, Sensor. Actuator. B Chem. 203 (2014) 102–110, https://doi.org/10.1016/j.snb.2014.06.076.

[4] N. Caicedo, R. Leturcq, J.P. Raskin, D. Flandre, D. Lenoble, Detection mechanism in highly sensitive ZnO nanowires network gas sensors, Sensor. Actuator. B Chem. 297 (2019) 126602, https://doi.org/10.1016/j.snb.2019.05.079.

[5] X. He, J.E. Yoo, M.H. Lee, J. Bae, Morphology engineering of ZnO nanostructures for high performance supercapacitors: enhanced electrochemistry of ZnO nanocones compared to ZnO nanowires, Nanotechnology 28 (2017) 245402, https://doi.org/10.1088/1361-6528/aa6bca.

[6] T. Voss, S.R. Waldvogel, Hybrid LEDs based on ZnO nanowire structures, Mater. Sci. Semicond. Process. 69 (2017) 52–56, https://doi.org/10.1016/j.mssp.2016.11.027.

[7] Z.L. Wang, Zinc oxide nanostructures: growth, properties and applications, J. Phys. Condens. Matter 16 (2004) 829–858, https://doi.org/10.1088/0953-8984/16/25/R01.

[8] Ü. Özgür, Y.I. Alivov, C. Liu, A. Teke, M.A. Reshchikov, S. Doğan, V. Avrutin, S.J. Cho, H. Morko, A comprehensive review of ZnO materials and devices, J. Appl. Phys. 98 (2005) 1–103, https://doi.org/10.1063/1.1992666.

[9] L.E. Greene, B.D. Yuhas, M. Law, D. Zitoun, P. Yang, Solution-grown zinc oxide nanowires, Inorg. Chem. 45 (2006) 7535–7543, https://doi.org/10.1021/ic0601900.

[10] A. Wibowo, M.A. Marsudi, M.I. Amal, M.B. Ananda, R. Stephanie, H. Ardy, L.J. Diguna, ZnO nanostructured materials for emerging solar cell applications, RSC Adv. 10 (2020) 42838–42859, https://doi.org/10.1039/d0ra07689a.

[11] C. Qiu, Y. Wu, J. Song, W. Wang, Z. Li, Efficient planar perovskite solar cells with ZnO electron transport layer, Coatings 12 (2022) 1981, https://doi.org/10.3390/COATINGS12121981.

[12] R. He, S. Nie, X. Huang, Y. Wu, R. Chen, J. Yin, B. Wu, J. Li, N. Zheng, Scalable preparation of high-performance ZnO–SnO2 cascaded electron transport layer for efficient perovskite solar modules, Sol. RRL 6 (2022) 2100639, https://doi.org/10.1002/SOLR.202100639.

[13] L. Lin, Z. Yang, E. Jiang, Z. Wang, J. Yan, N. Li, Z. Wang, Y. Ai, C. Shou, B. Yan, Y. Zhu, J. Sheng, J. Ye, ZnO-modified anode for high-performance SnO2-based planar perovskite solar cells, ACS Appl. Energy Mater. 2 (2019) 7062–7069, https://doi.org/10.1021/ACSAEM.9B00845.

[14] D. Wang, C. Wu, W. Luo, X. Guo, B. Qu, L. Xiao, Z. Chen, ZnO/SnO2 double electron transport layer guides improved open circuit voltage for highly efficient CH3NH3PbI3-based planar perovskite solar cells, ACS Appl. Energy Mater. 1 (2018) 2215–2221, https://doi.org/10.1021/ACSAEM.8B00293.

[15] M. Dkhili, G. Lucarelli, F. De Rossi, B. Taheri, K. Hammedi, H. Ezzaouia, F. Brunetti, T.M. Brown, Attributes of high-performance electron transport layers for perovskite solar cells on flexible PET versus on glass, ACS Appl. Energy Mater. 5 (2022) 4096–4107, https://doi.org/10.1021/ACSAEM.1C03311.

[16] J. Yang, B.D. Siempelkamp, E. Mosconi, F. De Angelis, T.L. Kelly, Origin of the thermal instability in CH3NH3PbI3 thin films deposited on ZnO, Chem. Mater. 27 (2015) 4229–4236, https://doi.org/10.1021/acs.chemmater.5b01598.

[17] Y. Cheng, Q.D. Yang, J. Xiao, Q. Xue, H.W. Li, Z. Guan, H.L. Yip, S.W. Tsang, Decomposition of organometal halide perovskite films on zinc oxide nanoparticles, ACS Appl. Mater. Interfaces 7 (2015) 19986–19993, https://doi.org/10.1021/acsami.5b04695.

[18] K. Schutt, P.K. Nayak, A.J. Ramadan, B. Wenger, Y.H. Lin, H.J. Snaith, Overcoming zinc oxide interface instability with a methylammonium-free perovskite for high-performance solar cells, Adv. Funct. Mater. 29 (2019) 1900466, https://doi.org/10.1002/adfm.201900466.

[19] M. Fahim, I. Firdous, W. Zhang, W.A. Daoud, Bifunctional interfacial engineering for piezo-phototronic enhanced photovoltaic performance of wearable perovskite solar cells, Nano Energy 86 (2021) 106127, https://doi.org/10.1016/J.NANOEN.2021.106127.

[20] G. Liu, Y. Zhong, H. Mao, J. Yang, R. Dai, X. Hu, Z. Xing, W. Sheng, L. Tan, Y. Chen, Highly efficient and stable ZnO-based MA-free perovskite solar cells via overcoming interfacial mismatch and deprotonation reaction, Chem. Eng. J. 431 (2022) 134235, https://doi.org/10.1016/J.CEJ.2021.134235.

[21] Y. Hu, T. Niu, Y. Liu, Y. Zhou, Y. Xia, C. Ran, Z. Wu, L. Song, P. Müller-Buschbaum, Y. Chen, W. Huang, Flexible perovskite solar cells with high power-per-weight: progress, application, and perspectives, ACS Energy Lett. 6 (2021) 2917–2943, https://doi.org/10.1021/ACSENERGYLETT.1C01193.

[22] D. Yang, R. Yang, S. Priya, S. (Frank) Liu, Recent advances in flexible perovskite solar cells: fabrication and applications, Angew. Chem. Int. Ed. 58 (2019) 4466–4483, https://doi.org/10.1002/ANIE.201809781.

[23] D. Yang, R. Yang, J. Zhang, Z. Yang, S. Liu, C. Li, High efficiency flexible perovskite solar cells using superior low temperature TiO2, Energy Environ. Sci. 8 (2015) 3208–3214, https://doi.org/10.1039/C5EE02155C.

[24] P. Kartikay, A. Yella, S. Mallick, All room-temperature-processed carbon-based flexible perovskite solar cells with TiO2 electron collection layer, Energy Technol. 10 (2022) 2200282, https://doi.org/10.1002/ENTE.202200282.

[25] B.J. Kim, D.H. Kim, Y.Y. Lee, H.W. Shin, G.S. Han, J.S. Hong, K. Mahmood, T.K. Ahn, Y.C. Joo, K.S. Hong, N.G. Park, S. Lee, H.S. Jung, Highly efficient and bending durable perovskite solar cells: toward a wearable power source, Energy Environ. Sci. (2015), https://doi.org/10.1039/c4ee02441a.

[26] F. Di Giacomo, V. Zardetto, S. Pescetelli, F. Matteocci, S. Razza, A. Di Carlo, S. Licoccia, W.M M Kessels, M. Creatore, T.M. Brown, F. Di Giacomo, S. Pescetelli, F. Matteocci, S. Razza, A. Di Carlo, T.M. Brown, V. Zardetto, W.M M Kessels, M. Creatore, S. Licoccia, Flexible perovskite photovoltaic modules and solar cells based on atomic layer deposited compact layers and UV-irradiated TiO2 scaffolds on plastic substrates, Adv. Energy Mater. 5 (2015) 1401808, https://doi.org/10.1002/AENM.201401808.

[27] V. Zardetto, T.M. Brown, A. Reale, A. Di Carlo, Substrates for flexible electronics: a practical investigation on the electrical, film flexibility, optical, temperature, and solvent resistance properties, J. Polym. Sci., Part B: Polym. Phys. 49 (2011) 638–648, https://doi.org/10.1002/POLB.22227.

[28] Y. Xu, Z. Lin, J. Zhang, Y. Hao, J. Ouyang, S. Liu, J. Chang, Flexible perovskite solar cells: material selection and structure design, Appl. Phys. Rev. 9 (2022) 021307, https://doi.org/10.1063/5.0084596.

[29] Y. Gao, K. Huang, C. Long, Y. Ding, J. Chang, D. Zhang, L. Etgar, M. Liu, J. Zhang, J. Yang, Flexible perovskite solar cells: from materials and device architectures to applications, ACS Energy Lett. 7 (2022) 1412–1445, https://doi.org/10.1021/acsenergylett.1c02768.

[30] Y. Xu, Z. Lin, W. Wei, Y. Hao, S. Liu, J. Ouyang, J. Chang, Recent progress of electrode materials for flexible perovskite solar cells, Nano-Micro Lett. 14 (2022) 1–30, https://doi.org/10.1007/S40820-022-00859-9, 2022 141.

[31] J. Zhang, W. Zhang, H.M. Cheng, S.R.P. Silva, Critical review of recent progress of flexible perovskite solar cells, Mater. Today 39 (2020) 66–88, https://doi.org/10.1016/j.mattod.2020.05.002.

[32] P. Rong, S. Ren, Q. Yu, Fabrications and applications of ZnO nanomaterials in flexible functional devices-A review, Crit. Rev. Anal. Chem. 49 (2019) 336–349, https://doi.org/10.1080/10408347.2018.1531691.

[33] K. Sekar, R. Nakar, J. Bouclé, R. Doineau, K. Nadaud, B. Schmaltz, G. Poulin-Vittrant, Low-temperature hydrothermal growth of ZnO nanowires on AZO substrates for FACsPb(IBr)3 perovskite solar cells, Nanomaterials 12 (2022) 2093, https://doi.org/10.3390/nano12122093.

[34] T.S. Tlemcani, C. Justeau, K. Nadaud, G. Poulin-Vittrant, D. Alquier, Deposition time and annealing effects of ZnO seed layer on enhancing vertical alignment of piezoelectric ZnO nanowires, Chemosensors 7 (2019) 7, https://doi.org/10.3390/CHEMOSENSORS7010007.

[35] C. Justeau, T.S. Tlemcani, G. Poulin-Vittrant, K. Nadaud, D. Alquier, A comparative study on the effects of Au, ZnO and AZO seed layers on the performance of ZnO nanowire-based piezoelectric nanogenerators, Materials 12 (2019) 2511, https://doi.org/10.3390/ma12162511.

[36] M. Xing, L. Wang, R. Wang, A review on the effects of zno nanowire morphology on the performance of interpenetrating bulk heterojunction quantum dot solar cells, Nanomaterials 12 (2022) 114, https://doi.org/10.3390/nano12010114.

[37] Ü. Özgür, V. Avrutin, H. Morkoç, Zinc oxide materials and devices grown by molecular beam epitaxy, Mol. Beam Ep. (2018) 343–375, https://doi.org/10.1016/b978-0-12-812136-8.00016-5.

[38] A.N. Baranov, P.S. Sokolov, V.L. Solozhenko, ZnO under pressure: from nanoparticles to single crystals, Cryst 12 (2022) 744, https://doi.org/10.3390/CRYST12050744, 2022, Vol. 12, Page 744.

[39] R. Kumar, O. Al-Dossary, G. Kumar, A. Umar, Zinc oxide nanostructures for no2 gas–sensor applications: a review, Nano-Micro Lett. 7 (2015) 97–120, https://doi.org/10.1007/s40820-014-0023-3.

[40] V. Consonni, A.M. Lord, Polarity in ZnO nanowires: a critical issue for piezotronic and piezoelectric devices, Nano Energy 83 (2021) 105789, https://doi.org/10.1016/J.NANOEN.2021.105789.

[41] S. Boubenia, A.S. Dahiya, G. Poulin-Vittrant, F. Morini, K. Nadaud, D. Alquier, A facile hydrothermal approach for the density tunable growth of ZnO nanowires and their electrical characterizations, Sci. Rep. 7 (2017) 15187, https://doi.org/10.1038/s41598-017-15447-w.

[42] A.S. Dahiya, S. Boubenia, G. Franzo, G. Poulin-Vittrant, S. Mirabella, D. Alquier, Photoluminescence study of the influence of additive ammonium hydroxide in hydrothermal grown ZnO nanowires, Nanoscale Res. Lett. 13 (2018) 249, https://doi.org/10.1186/s11671-018-2665-4.

[43] A. Galdámez-Martinez, G. Santana, F. Güell, P.R. Martínez-Alanis, A. Dutt, Photoluminescence of zno nanowires: a review, Nanomaterials 10 (2020) 857, https://doi.org/10.3390/nano10050857.

[44] A.S. Dahiya, C. Opoku, D. Alquier, G. Poulin-Vittrant, F. Cayrel, O. Graton, L.P.T. Huu Hue, N. Camara, Controlled growth of 1D and 2D ZnO nanostructures on 4H-SiC using Au catalyst, Nanoscale Res. Lett. 9 (2014) 1–9, https://doi.org/10.1186/1556-276X-9-379.

[45] N. Faraji, C. Ulrich, N. Wolff, L. Kienle, R. Adelung, Y.K. Mishra, J. Seidel, Visible-light driven nanoscale photoconductivity of grain boundaries in self-supported ZnO Nano- and microstructured platelets, Adv. Electron. Mater. 2 (2016) 1600138, https://doi.org/10.1002/aelm.201600138.

[46] M.A. Susner, S.D. Carnevale, T.F. Kent, L.M. Gerber, P.J. Phillips, M.D. Sumption, R.C. Myers, Catalyst-free ZnO nanowires on silicon by pulsed laser deposition with tunable density and aspect ratio, Phys. E Low-Dimensional Syst. Nanostructures. 62 (2014) 95–103, https://doi.org/10.1016/j.physe.2014.04.023.

[47] I. Isakov, M. Panfilova, M.J.L. Sourribes, P.A. Warburton, Growth of ZnO and ZnMgO nanowires by Au-catalysed molecular-beam epitaxy, Phys. Status Solidi Curr. Top. Solid State Phys. 10 (2013) 1308–1313, https://doi.org/10.1002/pssc.201200940.

[48] Z. Zheng, L. Gan, J.B. Zhang, F. Zhuge, T.Y. Zhai, An enhanced UV-Vis-NIR an d flexible photodetector based on electrospun Zno nanowire array/PbS quantum dots film heterostructure, Adv. Sci. 4 (2017) 1600316, https://doi.org/10.1002/advs.201600316.

[49] P. Kumari, A. Srivastava, R.K. Sharma, D. Sharma, S.K. Srivastava, Zinc Oxide: A Fascinating Material for Photovoltaic Applications, 2022, pp. 173–241, https://doi.org/10.1007/978-981-19-0553-7_6.

[50] A.S. Dahiya, F. Morini, S. Boubenia, C. Justeau, K. Nadaud, K.P. Rajeev, D. Alquier, G. Poulin-Vittrant, Zinc oxide nanowire-parylene nanocomposite based stretchable piezoelectric nanogenerators for self-powered wearable electronics, J. Phys. Conf. Ser. 1052 (2018) 012028, https://doi.org/10.1088/1742-6596/1052/1/012028.

[51] C. Opoku, A.S. Dahiya, C. Oshman, F. Cayrel, G. Poulin-Vittrant, D. Alquier, N. Camara, Fabrication of ZnO nanowire based piezoelectric generators and related structures, Phys. Procedia 70 (2015) 858–862, https://doi.org/10.1016/j.phpro.2015.08.176.

[52] C. Opoku, A.S. Dahiya, C. Oshman, C. Daumont, F. Cayrel, G. Poulin-Vittrant, D. Alquier, N. Camara, Fabrication of high performance field-effect transistors and practical Schottky contacts using hydrothermal ZnO nanowires, Nanotechnology 26 (2015) 355704, https://doi.org/10.1088/0957-4484/26/35/355704.

[53] C. Opoku, A.S. Dahiya, F. Cayrel, G. Poulin-Vittrant, D. Alquier, N. Camara, Fabrication of field-effect transistors and functional nanogenerators using hydrothermally grown ZnO nanowires, RSC Adv. 5 (2015) 69925–69931, https://doi.org/10.1039/c5ra11450k.

[54] A. Hamdi, A. Hamieh, M. Alamri, K. Dogheche, M.M.S. Mohan, R. Desfeux, D. Remiens, E. Dogheche, Morphological, structural, electrical, and piezoelectric analysis of hydrothermally grown ZnO nanowires on various substrates, Surface. Interfac. 31 (2022) 102103, https://doi.org/10.1016/j.surfin.2022.102103.

[55] E. Muchuweni, T.S. Sathiaraj, H. Nyakotyo, Low temperature synthesis of ZnO nanowires on GAZO thin films annealed at different temperatures for solar cell application, Mater. Sci. Semicond. Process. 68 (2017) 80–86, https://doi.org/10.1016/j.mssp.2017.06.011.

[56] J.S. Park, I. Mahmud, H.J. Shin, M.K. Park, A. Ranjkesh, D.K. Lee, H.R. Kim, Effect of surface energy and seed layer annealing temperature on ZnO seed layer formation and ZnO nanowire growth, Appl. Surf. Sci. 362 (2016) 132–139, https://doi.org/10.1016/j.apsusc.2015.11.193.

[57] K.A. Wahid, W.Y. Lee, H.W. Lee, A.S. Teh, D.C.S. Bien, I.A. Azid, Effect of seed annealing temperature and growth duration on hydrothermal ZnO nanorod structures and their electrical characteristics, Appl. Surf. Sci. 283 (2013) 629–635, https://doi.org/10.1016/j.apsusc.2013.06.159.

[58] M. Kam, Q. Zhang, D. Zhang, Z. Fan, Room-temperature sputtered SnO2 as robust electron transport layer for air-stable and efficient perovskite solar cells on rigid and flexible substrates, Sci. Rep. (2019) 1–10, https://doi.org/10.1038/s41598-019-42962-9, 2019 91. 9.

[59] A. Sławek, Z. Starowicz, M. Lipiński, The influence of the thickness of compact tio2 electron transport layer on the performance of planar ch3nh3pbi3 perovskite solar cells, Materials 14 (2021) 3295, https://doi.org/10.3390/MA14123295/S1.

[60] L.W. Ji, S.M. Peng, J.S. Wu, W.S. Shih, C.Z. Wu, I.T. Tang, Effect of seed layer on the growth of well-aligned ZnO nanowires, J. Phys. Chem. Solid. 70 (2009) 1359–1362, https://doi.org/10.1016/j.jpcs.2009.07.029.

[61] Y.K. Abeykoon, A.A.I. Lakmal, M.A.H.M. Munasinghe, B.S. Dassanayake, N. Gunawardhana, Optimization of seed layer thickness for the growth of the one dimensional vertically oriented ZnO nanowires, J. Mater. Sci. Mater. Electron. 34 (2023) 1–13, https://doi.org/10.1007/S10854-022-09657-W.

[62] W.Y. Wu, C.C. Yeh, J.M. Ting, Effects of seed layer characteristics on the synthesis of ZnO nanowires, J. Am. Ceram. Soc. 92 (2009) 2718–2723, https://doi.org/10.1111/j.1551-2916.2009.03022.x.

[63] Z.H. Azmi, S.N. Mohd Aris, S. Abubakar, S. Sagadevan, R. Siburian, S. Paiman, Effect of seed layer on the growth of zinc oxide nanowires by chemical bath deposition method, Coatings 12 (2022) 474, https://doi.org/10.3390/coatings12040474.

[64] B. Ikizler, S.M. Peker, Effect of the seed layer thickness on the stability of ZnO nanorod arrays, Thin Solid Films 558 (2014) 149–159, https://doi.org/10.1016/j.tsf.2014.03.019.

[65] J.N. Ding, Y.B. Liu, C.B. Tan, N.Y. Yuan, Investigations into the impact of various substrates and ZnO ultra thin seed layers prepared by atomic layer deposition on growth of ZnO nanowire array, Nanoscale Res. Lett. 7 (2012) 1–9, https://doi.org/10.1186/1556-276X-7-368.

[66] S. Guillemin, V. Consonni, E. Appert, E. Puyoo, L. Rapenne, H. Roussel, Critical nucleation effects on the structural relationship between ZnO seed layer and nanowires, J. Phys. Chem. C 116 (2012) 25106–25111, https://doi.org/10.1021/jp308643w.

[67] Y. Geng, K. Jeronimo, M.A. Bin Che Mahzan, P. Lomax, E. Mastropaolo, R. Cheung, Comparison of ZnO nanowires grown on e-beam evaporated Ag and ZnO seed layers, Nanoscale Adv. 2 (2020) 2814–2823, https://doi.org/10.1039/c9na00553f.

[68] A. Nourdine, M. Abdelli, N. Charvin, L. Flandin, Custom synthesis of zno nanowires for efficient ambient air-processed solar cells, ACS Omega 6 (2021) 32365–32378, https://doi.org/10.1021/acsomega.1c01654.

[69] Z. Han, S. Li, J. Chu, Y. Chen, Controlled growth of well-aligned ZnO nanowire arrays using the improved hydrothermal method, J. Semiconduct. 34 (2013) 063002, https://doi.org/10.1088/1674-4926/34/6/063002.

[70] M. Maddah, C.P. Unsworth, N.O.V. Plank, Selective growth of ZnO nanowires with varied aspect ratios on an individual substrate, Mater. Res. Express 6 (2019) 015905, https://doi.org/10.1088/2053-1591/aae6a2.

[71] A. Dymshits, L. Iagher, L. Etgar, Parameters influencing the growth of ZnO nanowires as efficient low temperature flexible perovskite-based solar cells, Materials 9 (2016) 60, https://doi.org/10.3390/ma9010060.

[72] W. Yang, Y. Wang, Q. Zhen, W. Shi, Effect of growth time on morphology and photovoltaic properties of ZnO nanowire array films, Rare Met. 30 (2011) 676–680, https://doi.org/10.1007/s12598-011-0448-5.

[73] I. Wallace, O.V. Eshu, O.B. Chukwunonso, U.C. Okoro, Synthesis and characterization of zinc oxide (ZnO) nanowire, J. Nanomed. Nanotechnol. 6 (2015) 321, https://doi.org/10.4172/2157-7439.1000321.

[74] A.F. Abdulrahman, S.M. Ahmed, S.M. Hamad, A.A. Barzinjy, Effect of growth temperature on morphological, structural, and optical properties of ZnO nanorods using modified chemical bath deposition method, J. Electron. Mater. 50 (2021) 1482–1495, https://doi.org/10.1007/S11664-020-08705-7.

[75] B. Weintraub, Z. Zhou, Y. Li, Y. Deng, Solution synthesis of one-dimensional ZnO nanomaterials and their applications, Nanoscale 2 (2010) 1573–1587, https://doi.org/10.1039/C0NR00047G.

[76] M.E. Coltrin, J.W.P. Hsu, D.A. Scrymgeour, J.R. Creighton, N.C. Simmons, C.M. Matzke, Chemical kinetics and mass transport effects in solution-based selective-area growth of ZnO nanorods, J. Cryst. Growth 310 (2008) 584–593, https://doi.org/10.1016/J.JCRYSGRO.2007.11.030.

[77] H. Tugral Arslan, C. Arslan, N. Baydogan, The effects of the curing parameters of the hydrothermal solution on the characteristic properties of ZnO nanowires, J. Opt. 51 (2022) 79–88, https://doi.org/10.1007/s12596-021-00757-0.

[78] V. La Ferrara, A. De Maria, G. Rametta, M. Della Noce, L.V. Mercaldo, C. Borriello, A. Bruno, P.D. Veneri, ZnO nanorods/AZO photoanode for perovskite solar cells fabricated in ambient air, Mater. Res. Express 4 (2017) 085025, https://doi.org/10.1088/2053-1591/aa7fcd.

[79] J. Qiu, X. Li, F. Zhuge, X. Gan, X. Gao, W. He, S.J. Park, H.K. Kim, Y.H. Hwang, Solution-derived 40νm vertically aligned ZnO nanowire arrays as photoelectrodes in dye-sensitized solar cells, Nanotechnology 21 (2010) 195602, https://doi.org/10.1088/0957-4484/21/19/195602.

[80] A. Eskandari, H. Abdizadeh, E. Pourshaban, M.R. Golobostanfard, An investigation into the role of polyethyleneimine in chemical bath deposition of zinc oxide nanowires, AIP Conf. Proc. 1920 (2018) 020026, https://doi.org/10.1063/1.5018958.

[81] A. Ul Hassan Sarwar Rana, M. Kang, H.S. Kim, Microwave-assisted facile and ultrafast growth of ZnO nanostructures and proposition of alternative microwave-assisted methods to address growth stoppage, Sci. Rep. 6 (2016) 1–13, https://doi.org/10.1038/srep24870, 2016 61.

[82] K. Liu, W. Wu, B. Chen, X. Chen, N. Zhang, Continuous growth and improved PL property of ZnO nanoarrays with assistance of polyethylenimine, Nanoscale 5 (2013) 5986–5993, https://doi.org/10.1039/c3nr00559c.

[83] R. Parize, J.D. Garnier, E. Appert, O. Chaix-Pluchery, V. Consonni, Effects of polyethylenimine and its molecular weight on the chemical bath deposition of ZnO nanowires, ACS Omega 3 (2018) 12457–12464, https://doi.org/10.1021/acsomega.8b01641.

[84] V. Gerbreders, M. Krasovska, E. Sledevskis, A. Gerbreders, I. Mihailova, E. Tamanis, A. Ogurcovs, Hydrothermal synthesis of ZnO nanostructures with controllable morphology change, CrystEngComm 22 (2020) 1346–1358, https://doi.org/10.1039/C9CE01556F.

[85] G. Amin, M.H. Asif, A. Zainelabdin, S. Zaman, O. Nur, M. Willander, Influence of pH, precursor concentration, growth time, and temperature on the morphology of ZnO nanostructures grown by the hydrothermal method, J. Nanomater. 2011 (2011), https://doi.org/10.1155/2011/269692.

[86] A.H. Rakhsha, H. Abdizadeh, E. Pourshaban, M.R. Golobostanfard, V.R. Mastelaro, M. Montazerian, Ag and Cu doped ZnO nanowires: a pH-Controlled synthesis via chemical bath deposition, Materialia 5 (2019) 100212, https://doi.org/10.1016/J.MTLA.2019.100212.

[87] L. Yang, J. Feng, Z. Liu, Y. Duan, S. Zhan, S. Yang, K. He, Y. Li, Y. Zhou, N. Yuan, J. Ding, S. Frank, L. Yang Liu, J. Feng, Z. Liu, Y. Duan, S. Zhan, S. Yang, K. He, Y. Li, Y. Zhou, F.) Liu, N. Yuan, J. Ding, Record-efficiency flexible perovskite solar cells enabled by multifunctional organic ions interface passivation, Adv. Mater. 34 (2022) 2201681, https://doi.org/10.1002/ADMA.202201681.

[88] H.S. Jung, G.S. Han, N.G. Park, M.J. Ko, Flexible perovskite solar cells, Joule 3 (2019) 1850–1880, https://doi.org/10.1016/J.JOULE.2019.07.023.

[89] J. Huang, H. Zhu, Y. Chen, C. Preston, K. Rohrbach, J. Cumings, L. Hu, Highly transparent and flexible nanopaper transistors, ACS Nano 7 (2013) 2106–2113, https://doi.org/10.1021/nn304407R.

[90] H. Zhu, Z. Xiao, D. Liu, Y. Li, N.J. Weadock, Z. Fang, J. Huang, L. Hu, Biodegradable transparent substrates for flexible organic-light-emitting diodes, Energy Environ. Sci. 6 (2013) 2105–2111, https://doi.org/10.1039/C3EE40492G.

[91] C. Yi, W. Li, S. Shi, K. He, P. Ma, M. Chen, C. Yang, High-temperature-resistant and colorless polyimide: preparations, properties, and applications, Sol. Energy 195 (2020) 340–354, https://doi.org/10.1016/J.SOLENER.2019.11.048.

[92] Y. Ma, Z. Lu, X. Su, G. Zou, Q. Zhao, Recent progress toward commercialization of flexible perovskite solar cells: from materials and structures to mechanical stabilities, Adv. Energy Sustain. Res. (2022) 2200133, https://doi.org/10.1002/AESR.202200133.

[93] J. Jin, D. Lee, H.G. Im, Y.C. Han, E.G. Jeong, M. Rolandi, K.C. Choi, B.S. Bae, Chitin nanofiber transparent paper for flexible green electronics, Adv. Mater. 28 (2016) 5169–5175, https://doi.org/10.1002/ADMA.201600336.

[94] M.H. Jung, N.M. Park, S.Y. Lee, Color tunable nanopaper solar cells using hybrid CH3NH3PbI3−xBrx perovskite, Sol. Energy 139 (2016) 458–466, https://doi.org/10.1016/J.SOLENER.2016.10.032.

[95] J.M. Burst, W.L. Rance, D.M. Meysing, C.A. Wolden, W.K. Metzger, S.M. Garner, P. Cimo, T.M. Barnes, T.A. Gessert, M.O. Reese, Performance of transparent conductors on flexible glass and plastic substrates for thin film photovoltaics, in: 2014 IEEE 40th Photovolt. Spec. Conf. PVSC 2014, 2014, pp. 1589–1592, https://doi.org/10.1109/PVSC.2014.6925223.

[96] S. Ke, C. Chen, N. Fu, H. Zhou, M. Ye, P. Lin, W. Yuan, X. Zeng, L. Chen, H. Huang, Transparent indium tin oxide electrodes on muscovite mica for high-temperature-processed flexible optoelectronic devices, ACS Appl. Mater. Interfaces 8 (2016) 28406–28411, https://doi.org/10.1021/ACSAMI.6B09166.

[97] S.M.F. Cruz, L.A. Rocha, J.C. Viana, S.M.F. Cruz, L.A. Rocha, J.C. Viana, Printing technologies on flexible substrates for printed electronics, Flex. Electron. (2018), https://doi.org/10.5772/INTECHOPEN.76161.

[98] K. Fukuda, K. Yu, T. Someya, The future of flexible organic solar cells, Adv. Energy Mater. 10 (2020) 2000765, https://doi.org/10.1002/AENM.202000765.

[99] L. Yang, Q. Xiong, Y. Li, P. Gao, B. Xu, H. Lin, X. Li, T. Miyasaka, Artemisinin-passivated mixed-cation perovskite films for durable flexible perovskite solar cells with over 21 % efficiency, J. Mater. Chem. A 9 (2021) 1574–1582, https://doi.org/10.1039/D0TA10717D.

[100] M.H. Kumar, N. Yantara, S. Dharani, M. Graetzel, P.P. Boix, N. Mathews, Flexible, low-temperature, solution processed ZnO-based perovskite solid state solar cells, Chem. Commun. 49 (2013) 11089–11091, https://doi.org/10.1039/C3CC46534A.

[101] G. Hu, W. Guo, R. Yu, X. Yang, R. Zhou, C. Pan, Z.L. Wang, Enhanced performances of flexible ZnO/perovskite solar cells by piezo-phototronic effect, Nano Energy 23 (2016) 27–33, https://doi.org/10.1016/J.NANOEN.2016.02.057.

[102] J. Sun, Q. Hua, R. Zhou, D. Li, W. Guo, X. Li, G. Hu, C. Shan, Q. Meng, L. Dong, C. Pan, Z.L. Wang, Piezo-phototronic effect enhanced efficient flexible perovskite solar cells, ACS Nano 13 (2019) 4507–4513, https://doi.org/10.1021/ACSNANO.9B00125.

[103] J. Nie, Y. Zhang, L. Li, Y. Zhang, High-performance piezophototronic solar cells based on polarization modulation perovskite, Adv. Devices Instrum. (2023), https://doi.org/10.34133/ADI.0025.

[104] F. Bouhjar, L. Derbali, B. Marí, High performance novel flexible perovskite solar cell based on a low-cost-processed ZnO:Co electron transport layer, Nano Res. 13 (2020) 2546–2555, https://doi.org/10.1007/S12274-020-2896-4, 2020 139.

[105] Y. Dkhissi, S. Meyer, D. Chen, H.C. Weerasinghe, L. Spiccia, Y.B. Cheng, R.A. Caruso, Stability comparison of perovskite solar cells based on zinc oxide and titania on polymer substrates, ChemSusChem 9 (2016) 687–695, https://doi.org/10.1002/CSSC.201501659.

[106] Y. Dong, J. Ma, S. Yang, H. Yang, Polyimides and their diverse applications in multiple optoelectronic devices, Adv. Devices Instrum. 4 (2023), https://doi.org/10.34133/ADI.0011.

[107] X. Liu, Y. Wang, G. Wang, Y. Ma, Z. Zheng, K. Fan, J. Liu, B. Zhou, G. Wang, Z. You, Y. Fang, X. Wang, S. Niu, An ultrasound-driven implantable wireless energy harvesting system using a triboelectric transducer, Matter 5 (2022) 4315–4331, https://doi.org/10.1016/J.MATT.2022.08.016.

[108] H.E. Unalan, P. Hiralal, D. Kuo, B. Parekh, G. Amaratunga, M. Chhowalla, Flexible organic photovoltaics from zinc oxide nanowires grown on transparent and conducting single walled carbon nanotube thin films, J. Mater. Chem. 18 (2008) 5909–5912, https://doi.org/10.1039/B810748C.

[109] K.H. Lee, B. Kumar, H.J. Park, S.W. Kim, Optimization of an electron transport layer to enhance the power conversion efficiency of flexible inverted organic solar cells, Nanoscale Res. Lett. 5 (2010) 1908–1912, https://doi.org/10.1007/S11671-010-9769-9.

[110] S. Chu, D. Li, P.C. Chang, J.G. Lu, Flexible dye-sensitized solar cell based on vertical ZnO nanowire arrays, Nanoscale Res. Lett. 6 (2011) 1–4, https://doi.org/10.1007/S11671-010-9804-X.

[111] D.Y. Kim, S. Lee, Z.H. Lin, K.H. Choi, S.G. Doo, H. Chang, J.Y. Leem, Z.L. Wang, S.O. Kim, High temperature processed ZnO nanorods using flexible and transparent mica substrates for dye-sensitized solar cells and piezoelectric nanogenerators, Nano Energy 9 (2014) 101–111, https://doi.org/10.1016/J.NANOEN.2014.07.004.

[112] Z. Li, G. Liu, Y. Zhang, Y. Zhou, Y. Yang, Porous nanosheet-based hierarchical zinc oxide aggregations grown on compacted stainless steel meshes: enhanced flexible dye-sensitized solar cells and photocatalytic activity, Mater. Res. Bull. 80 (2016) 191–199, https://doi.org/10.1016/J.MATERRESBULL.2016.04.005.

[113] M.K. Pathirane, W.S. Wong, Optical and electrical characteristics of hybrid ZnO nanowire/a-Si:H solar cells on flexible substrates under mechanical bending, Small 12 (2016) 2554–2558, https://doi.org/10.1002/SMLL.201503668.

[114] L. Zhu, L. Wang, F. Xue, L. Chen, J. Fu, X. Feng, T. Li, Z. Lin Wang, L. Zhu, L. Wang, F. Xue, L. Chen, J. Fu, T. Li, Z.L. Wang, X. Feng, Piezo-phototronic effect enhanced flexible solar cells based on n-ZnO/p-SnS core–shell nanowire array, Adv. Sci. 4 (2017) 1600185, https://doi.org/10.1002/ADVS.201600185.

[115] Y. Wang, W. Su, S. Zang, M. Li, X. Zhang, Y. Liu, Bending-durable colloidal quantum dot solar cell using a ZnO nanowire array as a three-dimensional electron transport layer, Appl. Phys. Lett. 110 (2017) 163902, https://doi.org/10.1063/1.4980136.

[116] S. Qiao, J. Liu, G. Fu, K. Ren, Z. Li, S. Wang, C. Pan, ZnO nanowire based CIGS solar cell and its efficiency enhancement by the piezo-phototronic effect, Nano Energy 49 (2018) 508–514, https://doi.org/10.1016/J.NANOEN.2018.04.070.

[117] S. Pathania, J.J.L. Hmar, B. Verma, T. Majumder, V. Kumar, P. Chinnamuthu, Titanium dioxide (TiO2) sensitized zinc oxide (ZnO)/Conducting polymer nanocomposites for improving performance of hybrid flexible solar cells, J. Electron. Mater. 51 (2022) 5986–6001, https://doi.org/10.1007/S11664-022-09815-0, 2022 5110.